Nano-Bilayer Lipid Membranes Hosted on Biogenic Nanoporous Substrates

by

Shankar Ramakrishnan

A Dissertation Presented in Partial Fulfillment
of the Requirements for the Degree
Doctor of Philosophy

Approved April 2015 by the
Graduate Supervisory Committee:

Michael Goryll, Chair
Jennifer Blain Christen
Sandwip Dey
Trevor Thornton

ARIZONA STATE UNIVERSITY

May 2015

ABSTRACT

Engineered nanoporous substrates made using materials such as silicon nitride or silica have been demonstrated to work as particle counters or as hosts for nano-lipid bilayer membrane formation. These mechanically fabricated porous structures have thicknesses of several hundred nanometers up to several micrometers to ensure mechanical stability of the membrane. However, it is desirable to have a three-dimensional structure to ensure increased mechanical stability. In this study, circular silica shells used from Coscinodiscus wailesii, a species of diatoms (unicellular marine algae) were immobilized on a silicon chip with a micrometer-sized aperture using a UV curable polyurethane adhesive. The current conducted by a single nanopore of 40 nm diameter and 50 nm length, during the translocation of a 27 nm polystyrene sphere was simulated using COMSOL multiphysics and tested experimentally. The current conducted by a single 40 nm diameter nanopore of the diatom shell during the translocation of a 27 nm polystyrene sphere was simulated using COMSOL Multiphysics (28.36 pA) and was compared to the experimental measurement (28.69 pA) and Coulter Counting theory (29.95 pA).In addition, a mobility of 1.11×10^{-8} $m^2s^{-1}V^{-1}$ for the 27 nm polystyrene spheres was used to convert the simulated current from spatial dependence to time dependence.

To achieve a sensing diameter of 1-2 nanometers, the diatom shells were used as substrates to perform ion-channel reconstitution experiments. The immobilized diatom shell was functionalized using silane chemistry and lipid bilayer membranes were formed. Functionalization of the diatom shell surface improves bilayer formation probability from 1 out of 10 to 10 out of 10 as monitored by impedance spectroscopy. Self-insertion of outer membrane protein OmpF of E.Coli into the lipid membranes could be confirmed using

single channel recordings, indicating that nano-BLMs had formed which allow for fully functional porin activity. The results indicate that biogenic silica nanoporous substrates can be simulated using a simplified two dimensional geometry to predict the current when a nanoparticle translocates through a single aperture. With their tiered three-dimensional structure, diatom shells can be used in to form nano-lipid bilayer membranes and can be used in ion-channel reconstitution experiments similar to synthetic nanoporous membranes.

Dedicated to my family and teachers

ACKNOWLEDGMENTS

I would like to take this opportunity to thank all the people who have contributed to my work and supported me in making this dissertation a reality. Firstly, I offer my sincere gratitude to my graduate advisor Dr. Michael Goryll, for accepting me as his Masters' and Doctoral student and giving me a chance to work under his guidance. His patience in dealing with my many questions and mistakes in innumerable situations has helped me to better understand the work that I am dealing with. He has been equally involved in all the experiments that we performed and this strengthened my confidence at times when I worked alone at the laboratory. He is an inspiration that pushes me to put in my best effort in whatever I do in this field and outside of it. Our interaction with each other for extended hours, both in the laboratory, or his office or over coffee has resulted in a fantastic working relationship which I am sure will continue in the future.

I would also like to thank Dr. Sandwip Dey for his valuable advice and spending time on discussing about the simulation. His time and efforts to discuss and edit my manuscript for the journal publication about the simulation was the most important reason that the manuscript was accepted.

I also would like to thank Dr. Trevor Thornton. My Masters' experience in the United States started with Dr. Thornton's class on the first day, which was crucial for the rest of my coursework and opinion about it. Taking his microelectronics course was a great experience and was instrumental in choosing the research work that I did. I am grateful to Dr. Jennifer Blain-Christen for accepting to be a member of my committee and her valuable feedback on my comprehensive presentation and future pathways. I would also like to

thank my lab partner and good friend Xiaofeng for the loads of coffee breaks that we took together.

My acknowledgement would be incomplete without mentioning the loving and caring family at Arizona in the form of The Faithful City at Tempe and all my mentors and friends here. Their support and advice has been instrumental in the successful completion of my work. No words can express my heartfelt gratitude to my parents and sister in India for their support and in listening to me over phone about diatoms and lipids. Without their support and belief in me none of this would have been ever possible.

TABLE OF CONTENTS

Page

LIST OF TABLES

LIST OF FIGURES

Figure Page

CHAPTER 1

INTRODUCTION

The focus of this research work is to study the use biogenic nanoporous substrates as a potential platform that can be used in applications that employ synthetic nanoporous membranes. The study is divided into two parts: 1) Simulation and testing of nanoparticle transport through biogenic nanopores and 2) Formation of lipid bilayer membranes across biogenic nanopores. This chapter begins with a background about the on-going and published research work in nanoparticle simulation and formation of nano-BLMs. It also describes the statement of research purpose and research questions.

1.1 Background

1.1.1 Coulter Counting

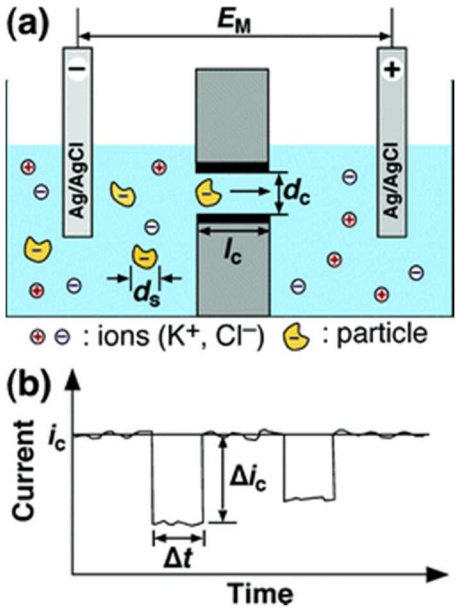

Figure 1: (a) Experimental setup for coulter counting (b) Current pulses obtained during a coulter counting experiment showing dwell time Δt and current pulse Δic (Henriquez 2004)

Coulter counter theory is based on the reduction in ionic current when a particle translocates within a channel. The value of the current decrease, or pulse height, can be used to determine the size of the particle, the width of the current pulse can be used to determine the charge carried by the particle, and the frequency of the current pulses can be used to determine the particle concentration.

The pulse height depends on the amount or volume of electrolyte solution that the particle displaces. This displacement of solution is represented by an increase in solution resistance locally. Once the particle has finished translocating through the channel the current returns to its baseline value as shown in Fig. 1b. The change in current due to the size of the particle is expressed by eqn. (1), which shows that the pulse height (Δic) is proportional to the third power of the diameter of the translocating spherical particle (ds).

$$\frac{\Delta i_c}{i_c} = S(d_c, d_s)\frac{d_s^3}{l_c' d_c^2} \quad \ldots (1)$$

S (d_c, d_s) is a correction factor that depends on the values of the channel diameter (d_c) and d_s. $l_{c'}$ is the corrected channel length for the so-called "fringe effect" ($lc' = lc + 0.8\ dc$). This means that smaller channels can be used to predict the current pulse height for smaller particles using this equation accurately.

The transport time is important in a Coulter counting experiment in case if the geometry of the channel is sufficiently well defined. The electrophoretic mobility of a particle, and hence its surface charge, can be determined. In the absence of specific chemical reactions between the particle and the channel there are four possible transport mechanisms that can contribute to the velocity of a particle through the channel. As shown in eqn. (2), these are

the velocities arising from pressure-driven flow (v_s, PD), electrophoresis (v_s, EP), electroosmosis (v_s, EO) and diffusion (v_s, D). In this Coulter counting experiment, diffusional transport is normally considered to be negligible, so only the other three terms need be considered.

$$v_s = v_{s,\,PD} + v_{s,\,EP} + v_{s,\,EO} + v_{s,\,D} = \frac{d_c^{\,2}}{32\eta l_{c'}}\Delta P + \frac{\mu}{l_{c'}}E_M + \frac{\varepsilon\zeta_c}{4\pi\eta l_{c'}}E_M + \frac{D_s}{l_c C_s}\Delta C_s \quad \ldots (2)$$

The width of the pulse signal (Δt) corresponds to the dwell time of a particle within the channel, and it provides the transport velocity of the particle (v_s) for a known length of the channel. In (2), η is the solution viscosity, ΔP is the pressure across the channel, μ is the electrophoretic mobility of the particle, ε is the solution dielectric constant, ζc is the zeta-potential of the channel surface, Ds is the diffusion coefficient of the particle, Cs is the particle concentration in the chamber containing the solution, and ΔCs is the difference between the particle concentrations in the two compartments.

In the previous discussion about the Coulter counter equation, the term involving pressure-driven flow was included. If Coulter counting is done based on electro kinetic transport, it can be easier to implement and can result in more information about the particle. In this case, both diffusion and pressure-driven flow can be considered negligible, and only electrophoresis and electroosmosis need to be considered. For channels that do not have well-defined geometries the effects of electroosmosis and electrophoresis cannot be distinguished, and therefore only information about particle size and concentration can be determined.

There are two approaches being pursued in research for the development of smaller, better-defined channels for Coulter counters. One of them uses self-assembled biological materials, and the other is based on mechanically fabricated channels. Each of these approaches has advantages that make it attractive for analyzing nanoscale objects. Out of these, we picked the biologically made nanoporous material from marine algae, diatoms.

1.1.2 Modeling

The electric field-induced translocation of nano-particles through nanopores with circular cross sections can be modeled using several approaches (Liu, Qian and Bau 2007). The coupled Nernst-Planck equations (multi-ion model, MIM) for the concentration fields of the ions in the solution and the Stokes equation for the liquid flow are solved simultaneously. The results from the multi-ion model were compared with the predictions from the Poisson-Boltzmann model (PBM) and the Smoluchowski's slip velocity model (SVM). The ion concentration field, the ionic current though the pore, and the particle's velocity were computed as functions of the particle's size, location, and electric charge; the pore's size and electric charge; the electric field intensity; and the bulk solution's concentration.

The Multi- ion model:

The multi-ion model (MIM) consists of the ion conservation equations, Poisson's equation, and the hydrodynamic equations for a viscous, incompressible fluid. Assuming

quasisteady state and no chemical reactions, the ionic conservation for species i requires that the flux (N_i) is divergence-free:

$$\nabla.\overrightarrow{N_\iota} = 0 \quad \ldots (3)$$

In the above,

$$\overrightarrow{N_\iota} = -D_i\nabla c_i - z_i m_i F c_i \nabla\emptyset + c_i\overrightarrow{u} \ldots . (4)$$

D_i is the molecular diffusion coefficient, c_i is the ionic concentration, m_i is the ion mobility, z_i is the valence, F is the Faraday constant, and u is the flow velocity. The first, second, and third terms in Eq. 4 correspond, respectively, to diffusion, migration, and convection. In the above, we assume that the diffusion coefficients and mobilities are uniform throughout the domain and neglect confinement effects.

The potential ϕ satisfies the Poisson equation where ε is the fluid's dielectric constant. Here, we assume that ε is uniform. The summation carried over K species represents the net charge density in the solution.

Since typically the Reynolds number associated with electrophoretic flows is very small, the inertial terms in the Navier-Stokes equation are neglected, the fluid motion is modeled with the Stokes equation,

$$\left[\eta\nabla^2 u - \nabla p - F\sum_{i=1}^{k} z_i c_i \nabla\emptyset\right] = 0 \ldots (5)$$

and the continuity equation for an incompressible fluid.

$$\nabla.\,\vec{u} = 0 \ldots (6)$$

In the above, p is the pressure and η is the fluid's dynamic viscosity. The first, second, and third terms in (5) represent, respectively, the viscous, pressure, and electrostatic forces.

To complete the mathematical model, the appropriate boundary conditions need to be specified. The boundary conditions associated with the electric field are $\phi(r, H) = \phi(r, -H) - \phi_0 = 0$, specified electric charge densities on the particle's and the membrane's surfaces, and insulation condition $\vec{n}.\nabla\emptyset = 0 \; at \; r = B$, where $\vec{n}$ is an outwardly-directed unit vector normal to the surface. The boundary conditions associated with the Nernst-Planck equation include specified concentrations at the top and bottom boundaries $c_i(r, H) = c_i(r, -H) = c_i^0$ and zero flux at all impermeable surfaces,

$$\overrightarrow{Ni}.\vec{n} = 0 \; \ldots (7)$$

The boundary conditions for the flow field are specified pressures at the top and bottom boundaries

$$p\,(r, H) = p\,(r, -H) = 0 \; \ldots (8)$$

zero velocities at all solid boundaries other than the particle's surface, and

$$\vec{u} = \; u_p.\overrightarrow{e_z} \; \ldots (9)$$

on the particle's surface. In the above, u_p is the vertical velocity of the particle's center of mass. The velocity u_p is determined by requiring the total force in the z direction (F_T) acting on the particle

$$F_T = \; F_E + \; F_D = 0 \; \ldots (10)$$

where,

$$F_E = \iint_S \sigma_P \,.\left(-\frac{\partial \emptyset}{\partial z}\right) dS \; \ldots (11)$$

$$F_D = -\iint_S (\mu \,.\left(\frac{\partial v}{\partial r} + \; \frac{\partial u}{\partial z}\right).n_r + (2\mu \frac{\partial v}{\partial z} - \; p).n_z) dS \; \ldots (12)$$

are, respectively, the electrostatic and hydrodynamic forces acting on the particle. S is the particle's surface; u and v are, respectively, the r and z components of $\vec{u}$; and n_r and n_z are, respectively, the r and z components of $\vec{n}$. In the above, it is assumed that the induced charges in the particle are negligible compared to the assigned surface charge σ_p.

The current density

$$\vec{\imath} = F\sum_{i=1}^{k} z_i(-D_i\nabla c_i - z_i m_i F c_i \nabla\emptyset + c_i\vec{u}) \ldots (13)$$

By integrating the (13) over the cross-sectional area of the pore, we obtain the total current through the pore.

The MIM predicts that, depending on the bulk solution's concentration, the translocating particle may either block or enhance the ionic current. In cases where the thickness of the electric double layer is relatively large, the PBM and SVM predictions do not agree with the MIM predictions.

1.1.3 Numerical Analysis

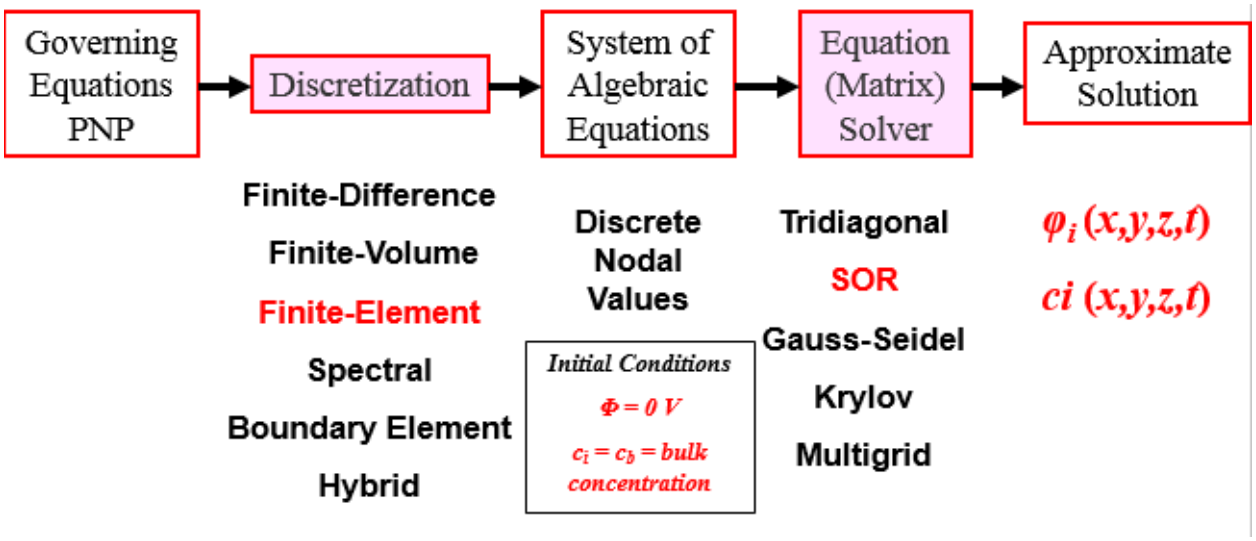

Figure 2: Solving methodology for solving the governing equations (Poisson- Nernst-Planck – Navier – Stokes) (Vasileska 2006)

The mathematical model for the simulation of the ionic current drop, using COMSOL multiphysics package accounts for the effects of applied electric field and convective flow of the electrolyte on the distribution of the ionic species. The overall methodology involves solving the Poisson's, Nernst-Planck, and Navier-Stokes equations using initial values of potential (ϕ), concentration (c_i) and flow velocity (u) in iterative steps to achieve convergence of these parameters at a specific position of the bead (Fig. 2). This procedure is repeated for various vertical positions of the bead within the aperture to calculate current using the surface integral of the current density across the aperture (Table 1).

The iterative procedure offered by COMSOL is conceptually similar to a conjugate gradient method. The Conjugate Gradient (CG) method is used to solve the finite-element form $\mathbf{Ax=b}$ of the partial differential equations used in the Poisson, Nernst-Planck and Navier-Stokes Equations. The basic methodology for a descent algorithm such as CG is: (1) start with an initial guess; (2) determine a direction of movement; (3) move in that direction to a relative minimum of the objective function; (4) determine a new direction and repeat the process. There are several types of algorithms that are based on the CG method. The rule by which successive directions of movement are selected differentiates these algorithms. For example, in the method of the steepest descent the initial guess is taken to be $x_{(0)}$ followed by a series of steps $x_{(1)}$, $x_{(2)}$,.. until a solution closest to the actual solution is achieved. The successive steps are determined by the direction in which the function f decreases rapidly as obtained from, $-f'(x_{(i)}) = b - Ax_{(i)}$. When the error between successive steps reaches a specified tolerance, convergence is said to have been achieved.

The tolerance can be increased or decreased to make the iterations faster or more accurate respectively.

Step	Process
1	Setup geometries of empty pore region with and without the nanoparticle as a 2D axisymmetric model and parameters and constants used in the Poisson – Nernst Planck and Navier Stokes' model
2	Setup triangular mesh with mesh size lesser than the Debye length of the solution
3	**Setup Poisson Solver :** $\boldsymbol{\nabla^2\emptyset = -\sum_i Fc_iz_i/\varepsilon}$
3a	*Electric potential V = 400 mV at solution boundary near pore entrance*
3b	*Ground at solution boundary near pore exit*
4	**Setup Nernst-Planck Solver:** $\boldsymbol{N_i = -D_i\nabla c_i - z_im_iFc_i\nabla\emptyset + c_iu}$
4a	*Concentration, c_b = 1 (mol/m^3) at solution boundary, mol/m^3*
5	**Setup Navier-Stokes Solver:** $\boldsymbol{u\nabla u = \frac{1}{\rho}[\eta\nabla^2 u - \nabla p - F\sum_i z_ic_i\nabla\emptyset]}$
5a	*Stationary wall, v = 0 along diatom surface, m/s*

Table 1: Multiphysics setup for solving the Multi-ion model iteratively

Further a study by White et al presents a study of nanoparticle transport in conical-shaped glass pores. The electrophoretic translocation of charged polystyrene nanoparticles (80 and 160-nm radius) were investigated using the Coulter counter principle. They recorded the time-dependent nanopore current as the polystyrene spheres were driven across the

membrane. Particle translocation through the conical-shaped nanopore causes a current that is dependent on the direction and a non-symmetric resistive pulse. Because of the presence of very high electric fields at the orifice, the translocation of nanoparticles through this area was very quick, that resulted in pulse widths of ~200 μs for the nanopores used in this study. A finite-element simulation was used to compute the position- and time-dependent nanoparticle velocity as the nanoparticle translocated through the conical-shaped nanopore. The positional results were used to compute the resistive pulse current-time response for conical-shaped pores, allowing comparison between experimental and simulated pulse heights and translocation times. The simulation and experimental results indicated that nanoparticle size can be differentiated based on pulse height, and to a lesser extent based on translocation time.

1.1.4 Nano-Bilayer Lipid membranes

The single channel ion channel reconstitution has been proven to be a reliable method in which bilayers are formed and ion channel proteins are self-inserted to observe and study their properties (Goryll 2009) (Hamill 1980) (Sakmann 1995) (S. Wilk 2005).

In the traditional method of 'painting', the thinning process of the bilayers that are formed is often unpredictable and the resulting bilayers may be fragile. In other cases the lipids may clump together forming a blob. In addition, the large scale of the system with bath volumes of several milliliters asks for a smaller sized system where the use of biological materials will not be excessive. This necessitates the use of smaller systems and a reliable method where lesser trials will be required to obtain a stable bilayer.

Applications of Nanopore Stochastic Sensing such as High Throughput Screening and 'Electronic Nose' require high sensitivity and discrimination with different affinities for analytes of interest (Zhao 2008). This can be achieved by an array of specific single channel sensors. The events are detected as transient blockades in the current that is recorded. The frequency of the event reveals the concentration of the analyte. The duration and amplitude reveal the identity of the element.

A number of platforms have been proposed for the arrangement of such an array and the recording of such signals in parallel. In most of these platforms an array of micro or nano-apertures is fabricated, which is used as the support for the lipid bilayer membranes that are formed. Ion channels are self-inserted into the bilayer membranes and the ionic current signal from these parallel sensors are recorded and then processed by DSPs.

Even if more than one ion channel is active in each bilayer formed, it still enables recording of single channel events in a parallel fashion, assuming that the amplifier resolution is sufficient.

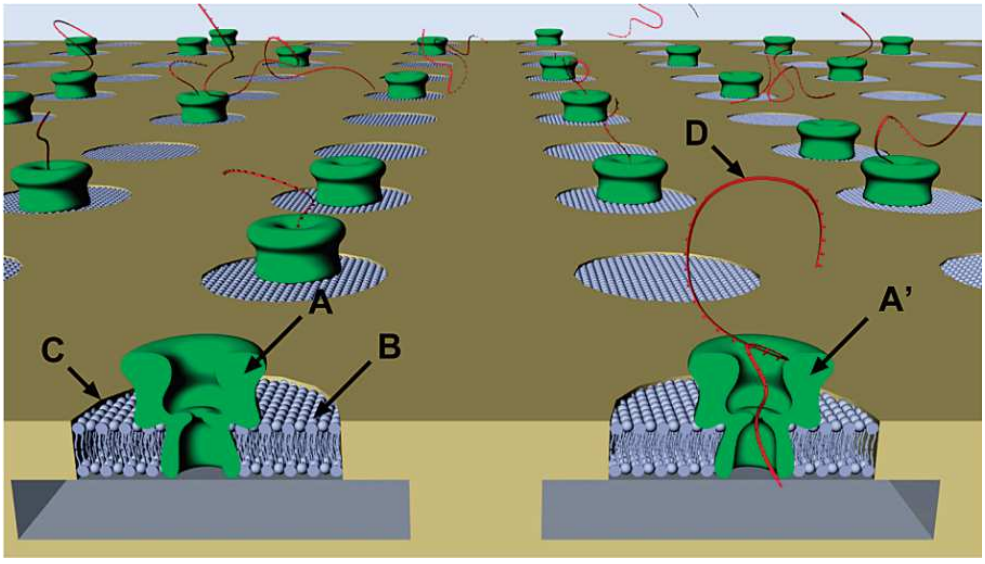

Figure 3: Parallel assay using α-Hemolysine nanopores (Osaki 2009)

A model of such a configuration is shown in Fig. 3. In this case a parallel assay is made simultaneously in chambers C, with lipid bilayers B. The bilayers have been reconstituted with the ion channels A and A'. The switching characteristic of the ion channels can subsequently be recorded in the absence and presence of a translocating molecule D respectively. In such a case it is important that each component sensor works independently of each other and is measured independently but also simultaneously.

Principal strategies for such reconstitution experiments include the formation of lipid bilayer membranes using bulk solutions or monolayers (Castellana 2006) followed by a thinning process (Niles 1988). Both these methods can be employed for the incorporation of ion channels into the bilayers requiring a site across which the bilayers can be hosted. In addition, specific ion channels have been engineered for RNA and DNA sequencing studies (Bayley and Cremer 2001) (Howorka and Siwy, Nanopore analytics: sensing of single molecules 2009) (Purnell and Schmidt, Discrimination of Single Base Substitutions in a DNA Strand Immobilized in a Biological Nanopore 2009) (Purnell, Mehta and Schmidt, Nucleotide identification and orientation discrimination of DNA Homopolymers immobilized in a protein nanopore 2008) (Butler, et al. 2008) (Howorka and Bayley, Probing distance and electrical potential within a protein pore with tethered DNA 2002). DNA strands can be sequenced by measuring the reduction in ionic current when they pass through such an engineered channel, which has to be hosted in a lipid bilayer membrane. Planar lipid bilayer membranes can be formed across micrometer-sized Teflon apertures to allow electrical recordings of ion channel proteins inserted into these membranes (Mayer, et al. 2003). Other substrates serving as suspended lipid bilayer membrane hosts are, silicon (S. Wilk 2005) or glass chips with micrometer sized apertures (White, et al. 2007)

(Castellana 2006). These membranes can be readily prepared and exhibit electrical seals in the gigaohm range. In addition, tethered bilayer membranes with good electrical sealing characteristics have been prepared (Krishna, et al. 2003) and reconstituted ion channels were inserted through them to measure ionic current flow (Atanasov, et al. 2005) (Andersson, et al. 2007) (Vockenroth, et al. 2008).

In this study, Nano – Bilayer Lipid membranes prepared using nano-meter sized porous apertures were reviewed. Two nanoporous materials that were considered for review from literature were porous alumina used by Steinem et al, and Silicon Nitride (Studer et al).

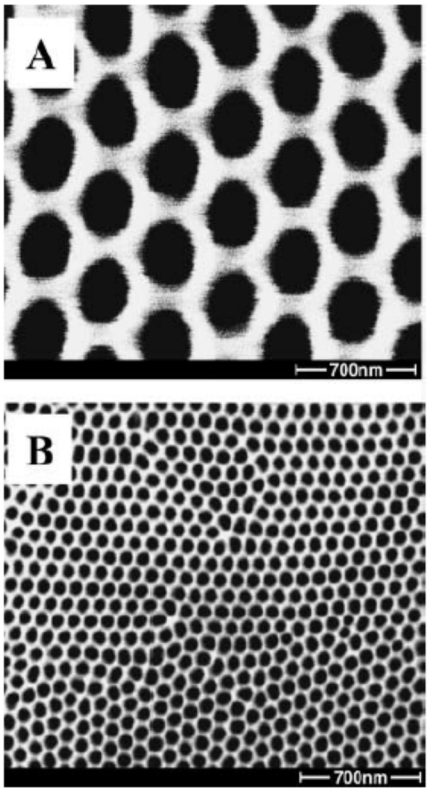

Figure 4: SEM micrographs (bottom views) of anodic alumina substrates with pore diameters (A) 280 nm and (B) 55 nm (Romer and Steinem, Impedance analysis and single-channel recordings on nano-black lipid membranes based on porous alumina 2004).

In the work done by Steinem et al, alumina pores with a diameter of 55 nm and 280 nm were used as supporting material for suspended lipid bilayer membranes (Fig. 4). The porous alumina was prepared by anodizing electro polished aluminum foils in aqueous oxalic acid (0.3 M) or phosphoric acid (5 wt. %). After the anodization process, aluminum was removed from the sample by incubating in $HgCl_2$ or acidulated $CuCl_2$. The resulting structure is an alumina porous structure with closed bottom pores. The closed bottom alumina layer was then removed using wet chemical etching in oxalic acid or phosphoric acid. The nanoporous alumina membrane was coated with gold using sputtering process. The gold surface was then made hydrophobic by incubating it in a solution of 1mM DPPTE in ethanol for 12 hours followed by washing it with ethanol and drying it in a stream of nitrogen.

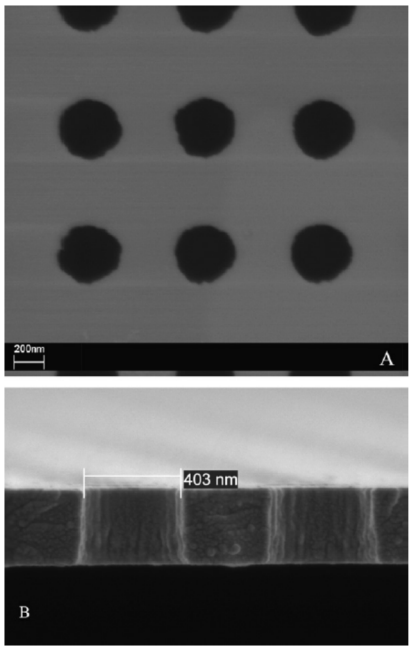

Figure 5: SEM images of the 400 nm Silicon Nitride chip by Studer et al from the surface (A) and of a cross-section (B) (Studer, et al. 2009)

The silicon nitride pores of sizes 200, 400 (Fig. 5) and 800 nm were prepared by Studer et al in a silicon nitride membrane of thickness 300 nm. Electron beam lithography was used for defining the pores. The pores are mentioned to be hydrophobic. However no information on how the pores were functionalized to be hydrophobic is known.

Both groups used bubble collapse method to form lipid bilayers across the nanopores. The aluminum nanopores were primed with lipids and dried in a stream of nitrogen before being inserted in a cis-trans chamber arrangement.

The results from Steinem et al show that a hydrophobic layer on the upper surface was a requirement for suspending nano-bilayer lipid membranes. The formation process and stability of the nano-BLMs were found to have increased. The lifetime was found to be close to 72 hours. The electrical impedance spectroscopy with typical specific membrane capacitances of (0.65 ± 0.2) $\mu F/cm^2$ and membrane resistances of up to 1.6 x 10^8 Ω cm^2. Single-channel recordings by inserting Gramicidin as well as alamethicin were conducted and they exhibited characteristic conductance states. Although Studer et al does not report any functionalization process to make it hydrophobic they do report an increased lifetime and formation of stable nano-lipid bilayer membranes.

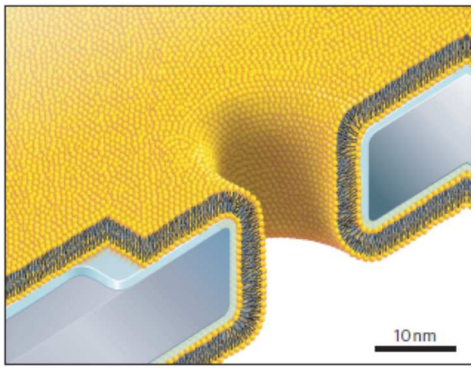

Figure 6: Drawing, to scale, showing a synthetic, lipid-coated (yellow) nanopore in a silicon nitride substrate (grey) and the interstitial water layer (blue). (Yusko 2011)

These studies indicate that a hydrophobic surface is essential for the formation of stable nano-bilayer lipid membranes. In further support of this hypothesis, the work done by (Yusko 2011) et al was studied. In this work lipid-bilayer-coated nanopores were created. To achieve this hydrophilic silicon chips with a single aperture through a silicon nitride window were exposed to an aqueous suspension of small unilamellar liposomes (Fig. 6). This process reduced the diameter of the nanopore by coating the surface with liposomes. The choice of lipids in the liposome preparation was used to control the thickness of the liposome coating. This further proves that lipids 'span' the aperture in a hydrophobic surface to form bilayer membranes whereas they 'line' or coat an unfunctionalized surface.

Lifetime and electrical seal in the gigaohm range were characteristics that were used to determine the quality of the lipid bilayer membranes formed in these studies. The stability of bilayers were found to be increased by decreasing the size of the bilayer membrane (Studer, et al. 2009) (L. X. Tiefenauer and A. Studer 2008). Nano-BLMs formed across 200 nm apertures in porous Silicon Nitride have been shown to exhibit an increased lifetime, by a factor of 30 when scaling the aperture diameter from 800 nm down to 200 nm (Studer, et al. 2009). Man-made nanoporous membranes are thus being explored as host for lipid bilayer membranes and subsequent ion-channel reconstitution experiments (Romer and Steinem, Impedance analysis and single-channel recordings on nanoblack lipid membranes based on porous alumina 2004) (Schmitt, Vrouenraets and Steinem 2006) (Gassmann, et al. 2009).

1.1.5 Biogenic nanoporous substrates – Diatom shells

The biogenic nanoporous substrates that were considered in this work were the algae called diatoms. Diatoms are single-celled algae that grow in seawater, freshwater, soil and damp surfaces. They are believed to be responsible to produce 25 % of the world's net organic carbon (Parkinson and Gordon 1999). The algae are unique in the feature that they are enclosed by a silica cell wall or shell that is porous. The extra-cellular silica shells are microscopic in size and can measure from 2 μm to 2 mm in diameter (Gordon and Drum, The chemical basis for diatom morphogenesis n.d.) (Fig .7). The shells are optically transparent and can be functionalized using silane chemistry (Yu, Addai-Mensah and Losic 2012) (Umemura, et al. 2007). The diatom shells are produced at an exponential rate on surfaces or in solution as opposed to a liner production rate in the case of man-made nanoporous substrates that are produced using lithography (Gordon, Losic, et al. 2009). In case of a man-made nanoporous substrate the design is man-made and can be controlled or modified in the fabrication process. There is a wide range of about 10^5 species of diatoms, which one can choose from, for a biogenic nanoporous substrate. In addition several modifications to the morphology can be done along with laboratory processes to change their characteristics. The wide range of structures available and the ease of modification processes that can be done to the diatom structure make it an attractive choice to employ in bottom-up nanoporous substrates.

Diatoms are classified into two major types based on the symmetry of the pores in the silica shell. Centric diatoms have a radial symmetry whereas pennate diatoms have rows of parallel pores arranged normal to the central axis (bilateral symmetry). The pores of

diatoms are arranged typically in a honeycomb structure possessing a high degree of symmetry. Aside from the symmetry, the diversity in structure and morphology offers several options for the choice of a substrate in nanotechnological applications.

As seen in several biological systems, the silica shell enclosing the biological material serves as a defense against predators and physical damage. The physical damage to the algae can be caused by abrasive particles and sediments. Other risks such as change in osmolarity can lead to bursting of unprotected cells. The silica shell or frustule consists of two valves that snap shut like petri dish shaped shells (Fig. 7) and are enclosed by girdle bands (Gordon, Losic, et al. 2009). As illustrated in Fig. 8, each shell consists of porous hexagonal chambers with a hierarchical plate-structure (Losic, Rosengarten, et al. 2006) (Parkinson and Gordon 1999). Each plate has uniform pore sizes with the pore sizes increasing or decreasing from the outer to the inner plate. The hierarchical plate structure lends mechanical stability to the structure. An inverse relationship between frustule size and mechanical strength has been reported in literature. It has been reported that stresses ranging from 150 to 680 N mm^{-1} were tolerated dependent upon the region where the force was applied (Losic, Mitchell and Voelcker, Diatomaceous lessons in nanotechnology and advanced materials 2009).

The circular *Coscinodiscus wailesii* was the diatom species chosen for this project. Since the lateral size of shells is about 250 μm (Boyd and Gradmann 1999), its placement at specific sites can be readily managed (Rapp 2004) (Kroeger and Poulsen 2008) (Bozarth, Maier and Zauner 2009) (Gordon, Losic, et al. 2009) (Lin, et al. 2010). The tiered plates are arranged with increasing pore sizes from the inner plate to the outer plate. The outermost plate has the finest pores of the order of 40 nm. The middle tier has pores of size

up to 120 nm and the innermost tier has the largest pores of size of up to 1100 nm. The pores lead to hexagonal chambers that are located between successive tiers. The tiered structure with increasing pore sizes helps the diatom provide selective entry to particle needed for its functioning. The tiered hierarchical structure along with the aspect ratio of pores with respect to the size of diatom shells makes the diatom shell an attractive alternative to man-made nanoporous substrates.

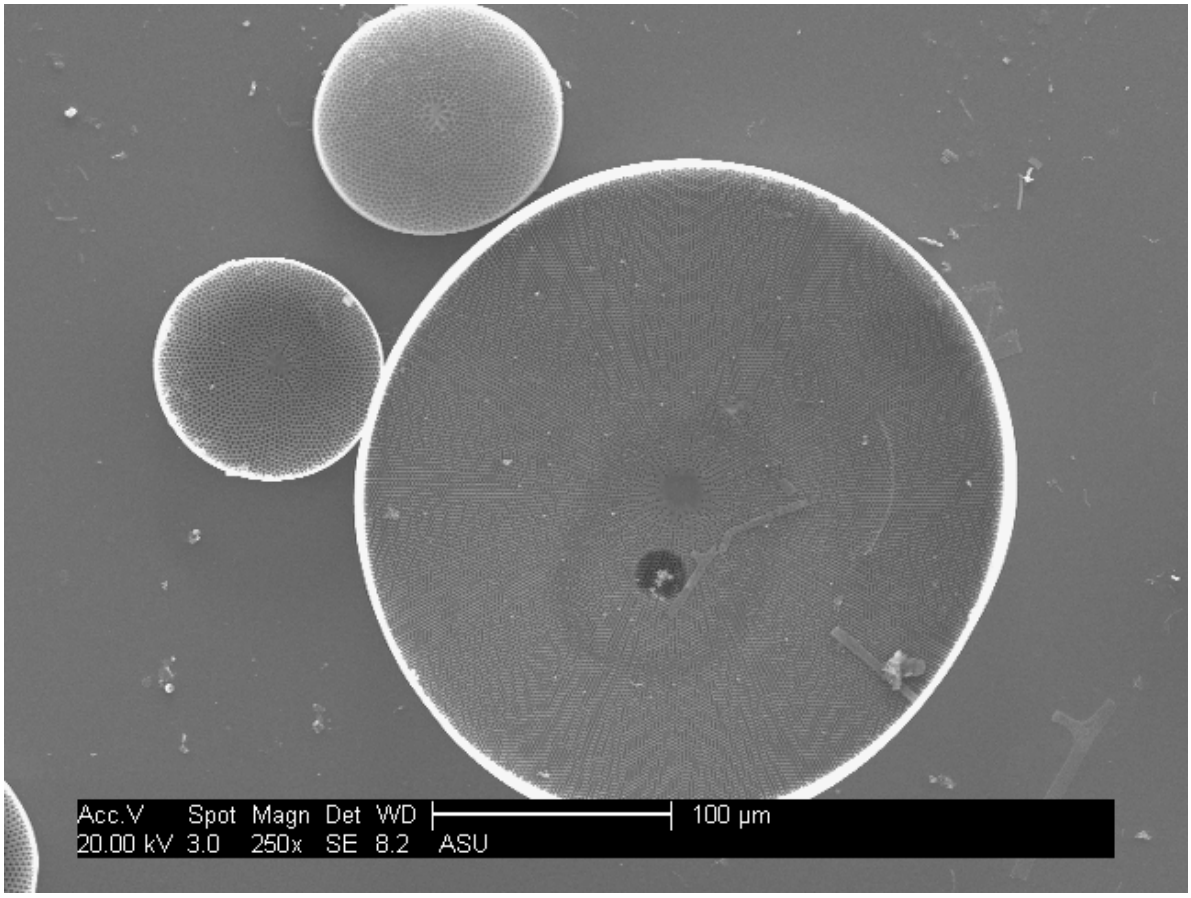

Figure 7: Scanning electron micrograph of diatom shells

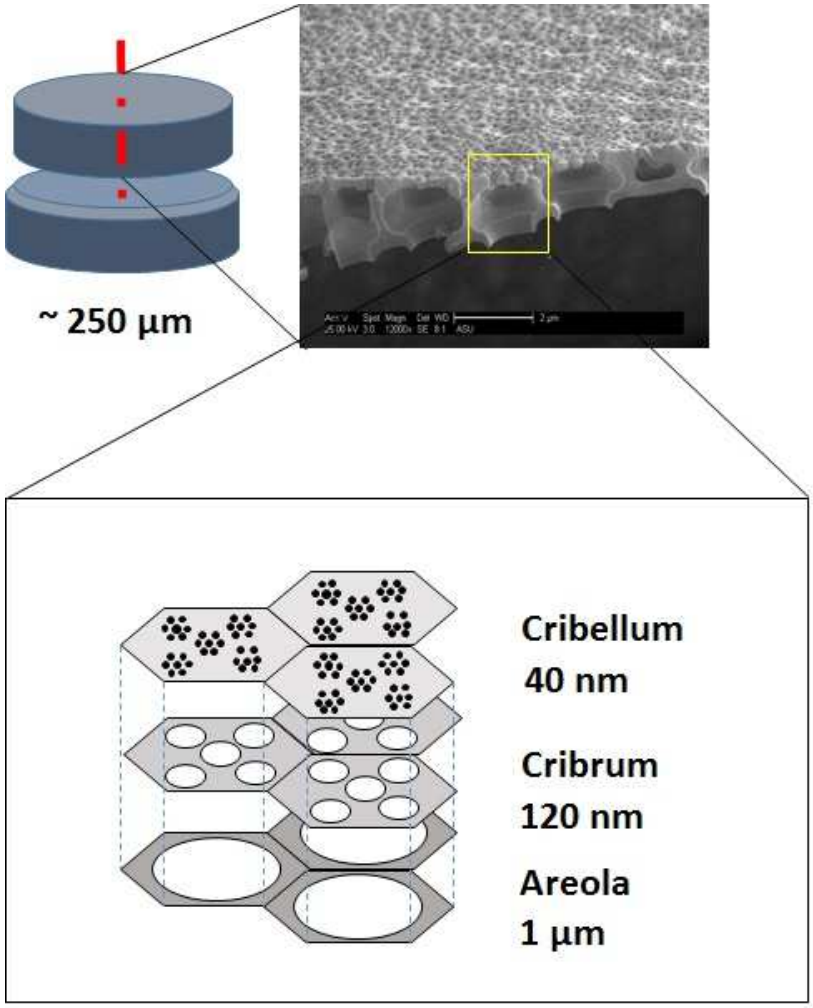

Figure 8: Illustration showing the tiered structure of a diatom shell

1.2 Statement of the research problem

Man-made nanoporous membranes are used in several medical applications (Adiga, et al. 2009) (Desai, et al. 1999) (Wee, et al. 2005) and molecular transport research (Nishizawa, Menon and Martin 1995) such as, sensing (Alfredo de la Escosura-Muñiz and Merkoçi 2012), separation (Striemer, et al. 2007), drug-testing (Prasad and Quijano 2006) and cell-cultures (Takoh, et al. 2005) (Agrawal, et al. 2010) (Khung, Barritt and Voelcker 2008). Silicon nitride (Vlassiouk, Apel, et al. 2009), alumina (Romer and Steinem,

Impedance analysis and single-channel recordings on nano-black lipid membranes based on porous alumina 2004) (Jani, et al. 2008) and silica (Jane, et al. 2009) are popular materials used in the production of these membranes.

Alumina is easy to use in fabrication processes and is also a biocompatible material (Ward, et al. 1997) A two-step anodization process is used in preparation of alumina nanopores (G. 2002) (Masuda, et al. 1997) in an acidic solution of sulfuric, phosphoric or oxalic acid. The membranes are removed from the supporting metal by dissolving the metal in dilute hydrochloric acid, or incubating in mercuric chloride or acidulated copper chloride. The pore size and distribution of pores are controlled using the etch conditions (Coakley, et al. 2005). Nanopore arrays with sizes ranging from 15 nm to 300 nm can be produced based on the amount of etch current applied (Coakley, et al. 2005) (Prasad and Quijano 2006).

Silicon-based substrates are increasingly being used to allow for electronic integration and scaling down of size (Jane, et al. 2009). Porous silica substrates are prepared using processes such as focused ion beam (Komarov, et al. 2005), electron beams (Lo, Aref and Bezryadin 2006) (Wu, et al. 2005) (Kim, et al. 2006), sol – gel process (Kra¨mer, et al. 1998) and ion-track etching (Vlassiouk, Apel, et al. 2009). In a large volume setting these techniques prove to be slow. Additionally, while these membranes can be easily varied in thickness, they often exhibit stress, leading to curvature and eventual breakage of the nanopore membrane.

It is evident that commercially available nanoporous membranes need to be thick for mechanical stability, from hundreds of nanometers up to several micrometers. In order to maintain a low aspect ratio of the nanopores, a tiered structure would be necessary to

stabilize the nanopore membrane structure (Schumann, et al. 2009). However, a nanoporous structure with small pore size and tiered structure would be a challenge to produce with a top-down approach. An alternate solution that can be used with a bottom-up approach is needed.

1.3 Statement of the purpose

The purpose of this study was to explore the possibility of using biogenic nanoporous substrates as a platform using a bottom – up approach. Biogenic nanoporous substrates with small pore sizes and a tiered structure are expected to be used in sensing applications, with the capability to predict the coulter current using simplified simulation techniques. In addition the nanoporous structure is expected to host an arrayed structure of nano bilayer lipid membranes (nano BLMs) across the substrate.

1.4 Research Questions

This research was undertaken to answer four questions on the possibility of using biogenic porous substrates as a potential platform that can compete with man-made nanoporous substrates.

1. Can a nanoporous geometry be modeled using a simplified geometry to simulate a translocating particle?
2. What is the probability of forming nano-BLMs across a biogenic nanoporous substrate?
3. What factors affect the nano-BLM formation?
4. How can the biogenic substrate be placed on the test platform?

CHAPTER 2

METHODS

2.1 Simulation

A simple 2D axisymmetric model of the diatom pore with diameter 40 nm and length 50 nm was developed and meshed using COMSOL Multiphysics package (Fig. 9). The Poisson-Nernst-Planck model was used in combination with the Navier-Stokes equation to set up the model physics (Liu, Qian and Bau 2007) (Jubery, et al. 2012) (Vlassiouk, Smirnov and Siwy, Ionic Selectivity of Single Nanochannels 2008).

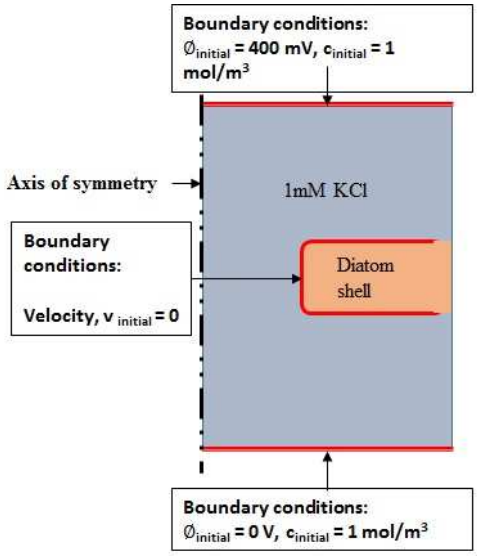

Figure 9: COMSOL multiphysics model showing the geometry of a single nanopores and initial conditions

The multi-physics geometry was setup using an approximate figure of a single nanopores from the diatomaceous shell. As shown in Fig. 10 the setup was a 2D- axisymmetric figure

which when rotated around the z- axis produces a 3D representational geometry of the single nanopore. Converting a 2D axi-symmetric geometry into a 3D geometry has two advantages: i) reduced computational time and iterative steps ii) Less use of computational resources speeding up computational time further and reducing geometric complexity to achieve convergence of iteration.

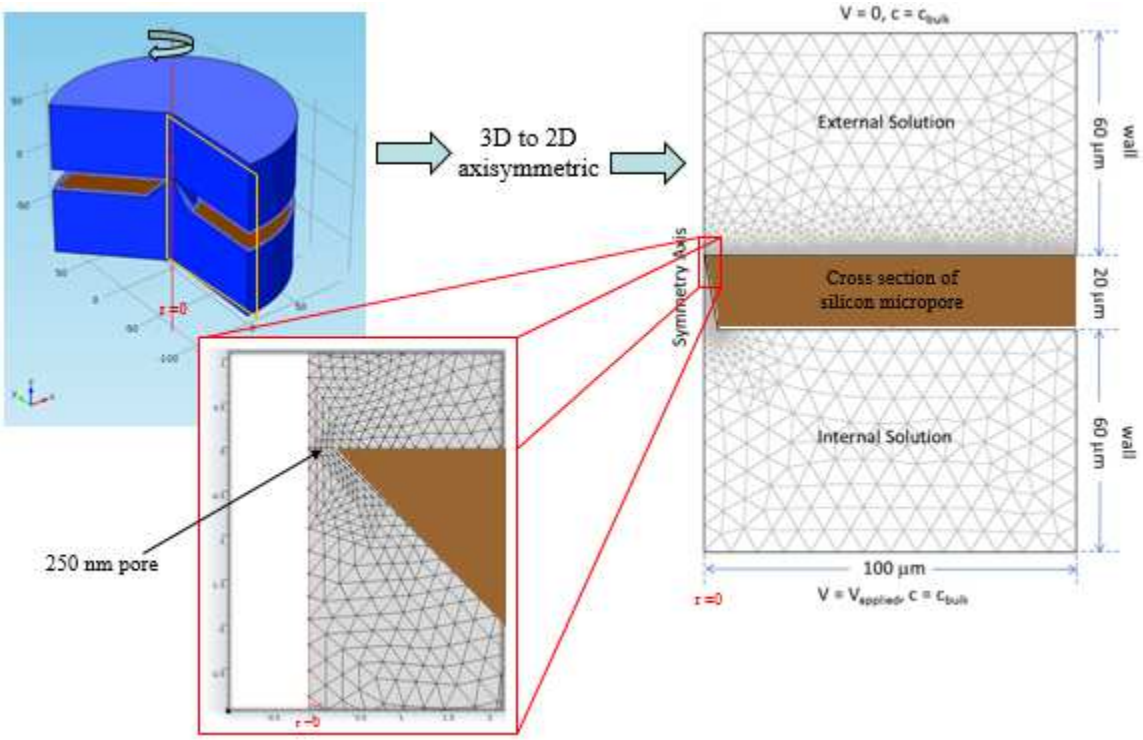

Figure 10: 2D – axisymmetric COMSOL model of a single nanopores with sharp edge converted from a 3D structure

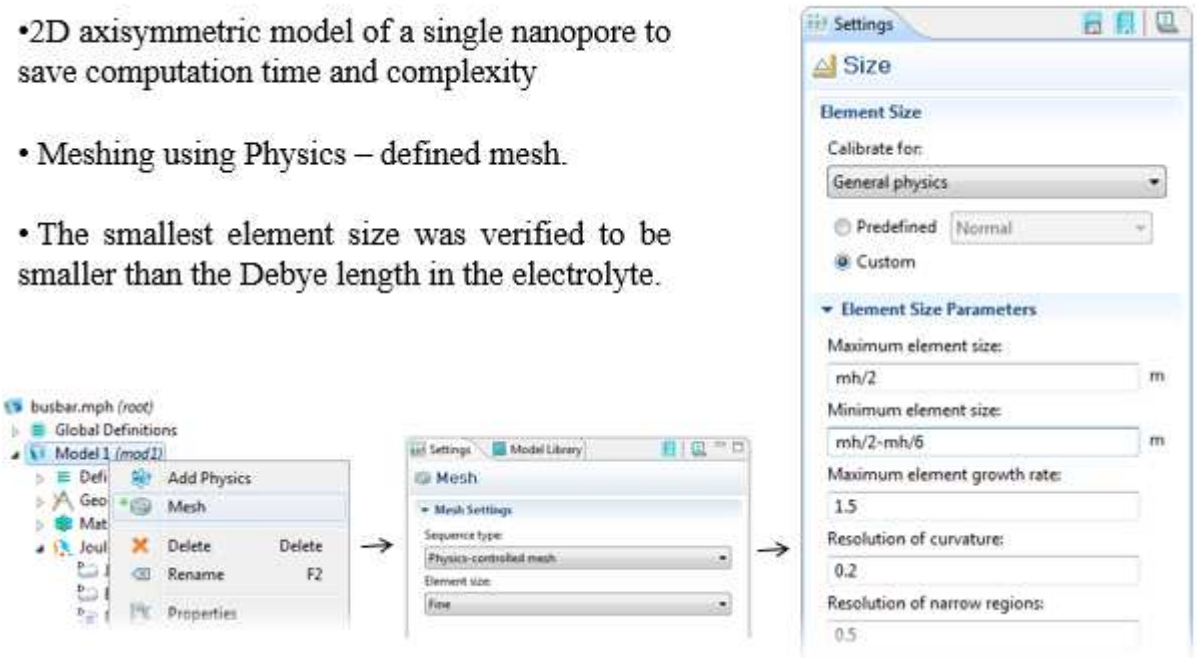

Figure 11: Meshing setup in COMSOL Multiphysics

Three modules were added to the physics that needs to be solved for the geometric model:

Electrostatics Module (es) for Poisson Equation

Transport of Dilute Species Module (chds) for Nernst – Planck Equation

Laminar Flow Module (spf) for Navier Stokes Equation

The models were coupled through the following variables:

Concentration of the ionic species (c1 for K^+ and c2 for Cl^-)

Voltage, V

Z component of Electric field, Ez

Velocity of flow, u.

To determine the current through the aperture, the initial electric field is determined from the Poisson's equation:

$$\nabla^2 \emptyset = -\sum_i F c_i z_i / \varepsilon \ \ldots (14)$$

where, $\emptyset$ is the potential at a node, F is the Faraday constant, c_i is the concentration of each ionic specie, i, in the solution, z_i is the charge number (+1 or -1), and ε is the uniform dielectric permittivity of the ionic solution. The boundary conditions are as follows: (i) applied voltage $\emptyset_0$ at the top and zero voltage (ground) at the bottom boundaries (see Fig. 12), (ii) surface charge densities on the particle and aperture surfaces are assumed to be zero.

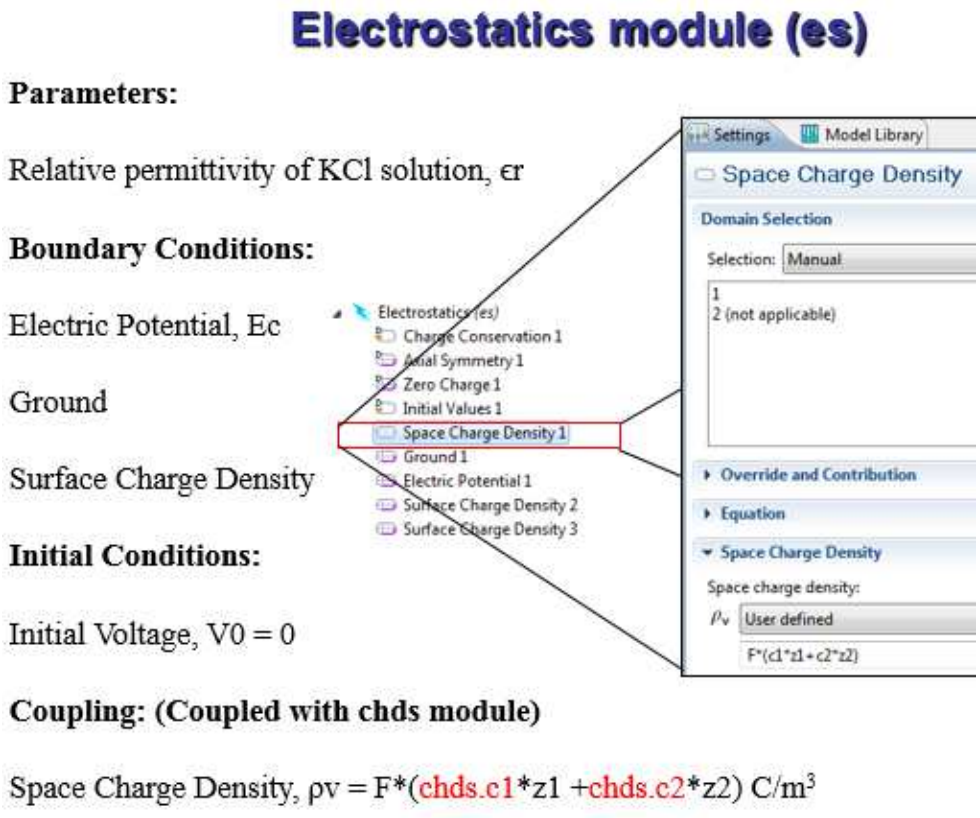

Figure 12: Electrostatics (es) module: Initial conditions, boundary conditions and coupling variable setup

Next, in the dilute solution approximation, the flux of each ionic species is calculated using the Nernst-Planck equation that describes diffusion and migration in an external electric field (i.e., $-\nabla\emptyset$ as determined previously) as follows:

$$N_i = -D_i\nabla c_i - z_i m_i F c_i \nabla\emptyset + c_i u \ldots (15)$$

where, $\nabla . N_i = 0$ for ionic conservation, assuming quasi-steady state. N_i, D_i and m_i are the flux, the diffusion coefficient, ion mobility, respectively, for each ionic specie and u is the flow velocity. Note, the first, second and third terms in the equation correspond to diffusion, migration and convection, respectively. Here, the boundary conditions are as follows: (i) concentrations at the top and bottom boundaries, cb = 1 mM KCl and (ii) Ni = 0 in impermeable surfaces (Fig. 13). The diffusion coefficients (DK+ of 1.957 x 10^{-9} m^2/s, DCl- of 2.032 x 10^{-9} m^2/s) and ion mobilities (μK+ of 7.619 x 10^{-8} $m^2s^{-1}V^{-1}$, μCl- of 7.912 x 10^{-8} $m^2s^{-1}V^{-1}$) are assumed to be uniform throughout the system.

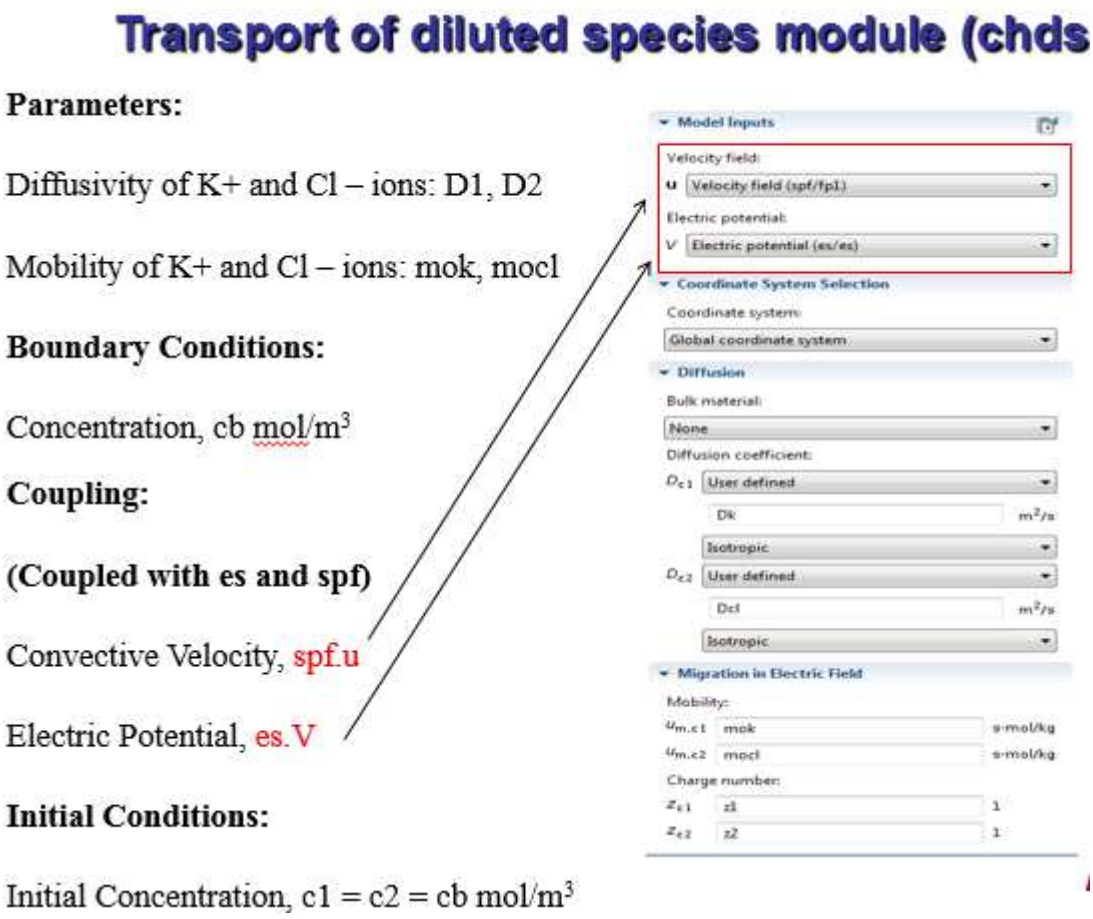

Figure 13: Transport of dilute species (chds) module: Initial conditions, boundary conditions and coupling variables setup

The flow velocity in the Nernst-Planck equation is determined from the Stokes equation as follows:

$$u\nabla u = \frac{1}{\rho}[\eta\nabla^2 u - \nabla p - F\sum_i z_i c_i \nabla\emptyset] \quad \ldots (16)$$

where, $\nabla . u = 0$, continuity equation for an incompressible fluid. η is the dynamic viscosity, ρ is the density, and p is the pressure. Note, (16) is a balance of momentum from Newton's second law. Here, the boundary conditions for Stokes equation are as follows: (i) atm

pressure at the top and bottom boundaries, (ii) zero velocity at all surfaces except the nanoparticle surface and (iii) nanoparticle velocity, $u_b = \mu_b . e_z$, where μb is the mobility of the nanoparticle and ez is the electric field (i.e., $-\nabla\emptyset_z$) in the direction of motion (Fig. 14).

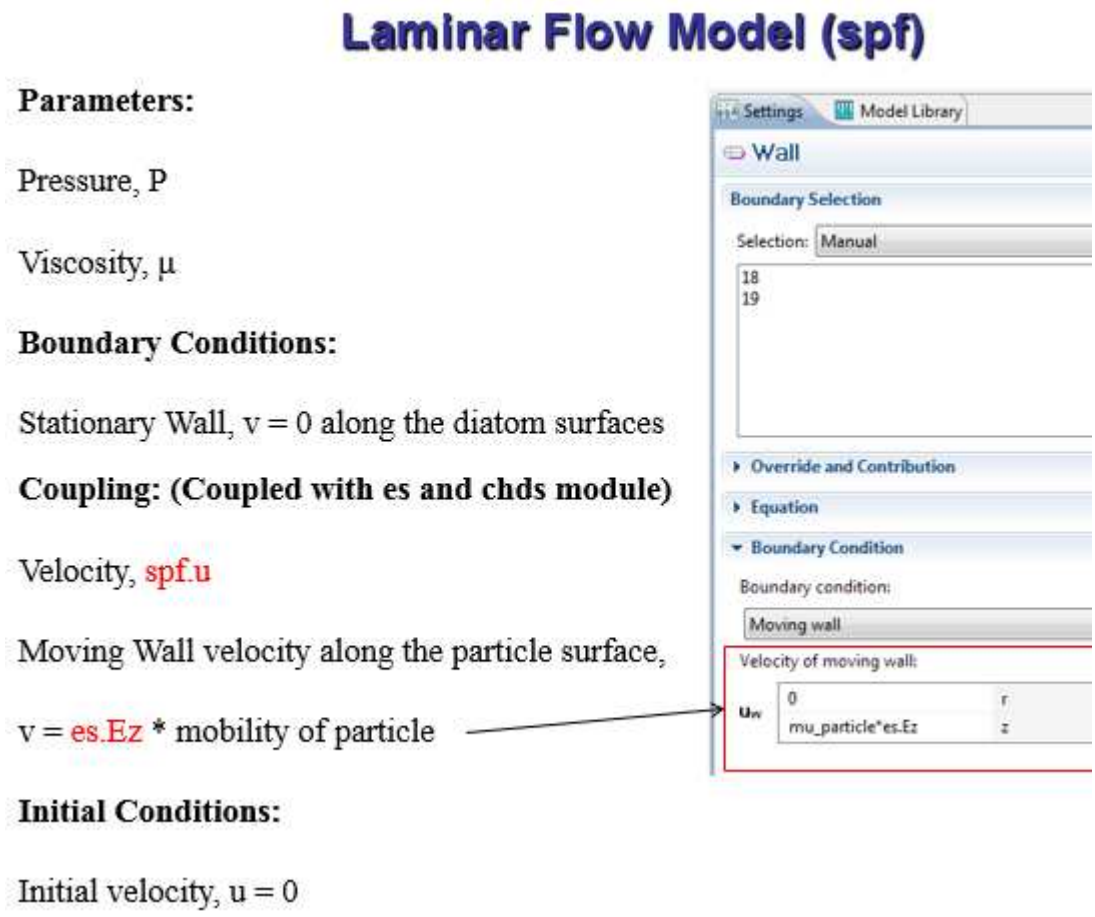

Figure 14: Laminar Flow (spf) module: Initial conditions, boundary conditions and coupling variable setup

The three equations are coupled by the parameters,$\emptyset$, c_i and u. The current through the open pore was calculated using

$$i = F\sum_i z_i(-D_i\nabla c_i - z_i m_i F c_i \nabla\emptyset + c_i u) \ldots (17)$$

The pore geometry was meshed with a triangular mesh with mesh size lesser than the Debye length in the ionic solution. The ionic solution was 1mM potassium chloride at pH 7.4 and the particle size was 27 nm. The diffusivity of the ionic species was taken to be $D_{K^+} = 1.957 \times 10^{-9}$ m^2/s and $D_{Cl^-} = 2.032 \times 10^{-9}$ m^2/s with a dielectric constant of 80. The 'open – pore' simulation was carried out in an iterative procedure with converging solutions in each iteration. The flow diagram of the procedure is shown in Fig. 16.

To obtain the translocation current, a particle was introduced in the geometry at twelve positions along its motion through the pore (Fig. 15). At each position of the particle, the simulation was executed and the current through the pore was calculated using the surface integral of the current density across the pore.

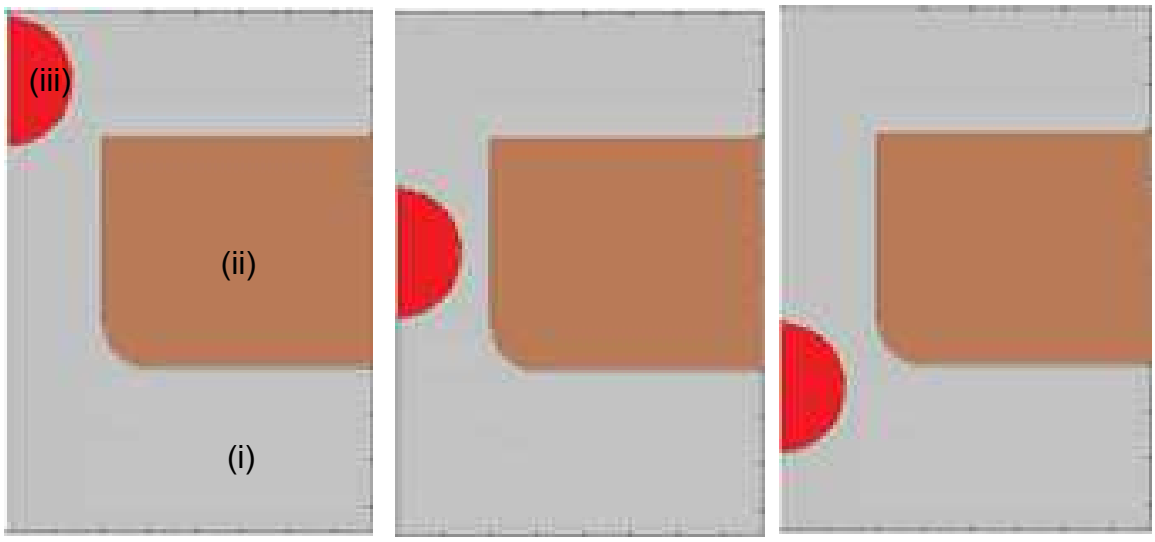

Figure 15: Simulation models of the nanoparticle inside the pore at different positions. The regions marked (i), (ii) and (iii) correspond to the ionic solution in the pore, silica shell and the translocating particle respectively.

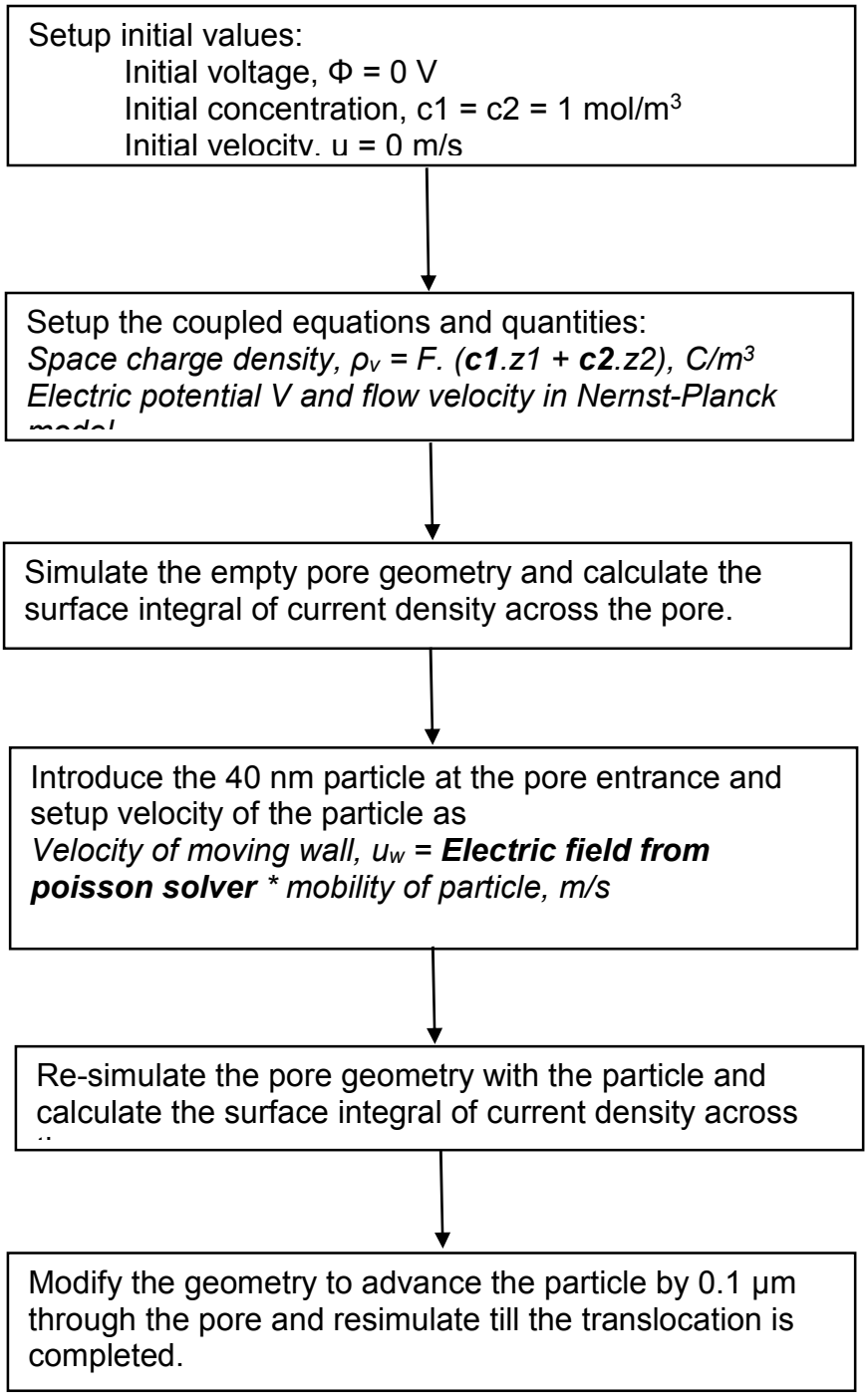

Figure 16: Procedure to solve the Poisson - Nernst Planck and Navier Stokes model using COMSOL multiphysics

2.2 Diatom Culture

The circular shaped diatoms *Coscinodiscus wailesii* and f/2 medium to enrich the seawater were ordered from the National Center for Marine Algae and Microbiota (NCMA). The diatoms were cultured in f/2 seawater medium at 20 ˚C under continuous photoperiod in a sterile environment (Losic, J.G. and Voelcker, Diatom culture media contain extracellular silica nanoparticles which form opalescent films 2008). The diatoms were cleaned by the addition of 50% (v/v) hydrogen peroxide (30% solution) and incubated at 90 ◦C for 1–2 hours, to remove organic materials. The shells were centrifuged at 3000 rpm for 5 min, and washed several times with nanopure water, and stored in 70% ethanol solution. At the end of this treatment, the diatom shell separates into two frustule valves and a girdle band. The frustule valves were separated from the girdle band and small debris using the settling method (Zhang, Wang and Pan 2010).

2.3 Micro-machined Silicon support

The silicon support structure (Fig. 17) was prepared using 4" diameter, double-sided polished Si (1 0 0) wafers with a thickness of 400 µm. A 100 µm diameter aperture was patterned and developed. A modified Bosch process was used to etch the silicon thinning the 100 µm diameter patterned region to a final thickness of 40µm (Wilk, Goryll, et al. 2004) (S. J. Wilk, et al. 2007). In a subsequent step, the through-wafer via aperture with a diameter of 30 µm was defined and the Bosch process was employed again to create the through-wafer aperture. The micro machined silicon substrate was thermally oxidized

to provide electrical insulation and an oxide surface for subsequent chemical modification. Next, SU-8 3025 UV-pattern able negative tone epoxy resin was spun on the large recess side and exposed to open up the recess structure. The 40 µm thick epoxy layer reduces the capacitance of the silicon chip in a fluidic cell, thereby reducing the electrical noise originating from the setup. The wafer was then diced into 1 cm by 1 cm individual pieces each holding a single aperture.

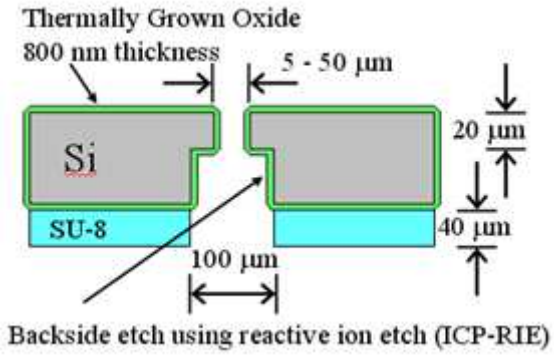

Figure 17: Cross-sectional illustration of the micro-machined silicon support

2.4 Placement and Immobilization of diatom shells on silicon chip

Poly-L-Lysine (0.1 % in deionized water) is coated on the surface of the silicon surface for better adherence of the diatom shell that was placed subsequently. A diatom shell was positioned over the 30 µm aperture in the silicon substrate, using a micromanipulator (Fig. 18). After positioning the diatom shell immobilization can be performed by two methods: a) Immobilization using NOA 60 UV curable photopolymer and b) Sintering process

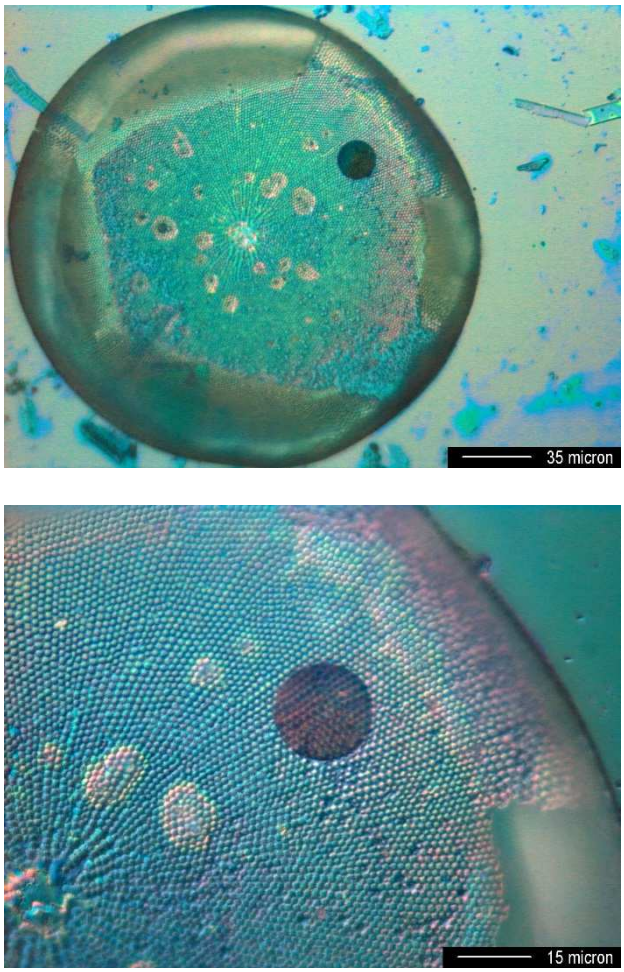

Figure 18: Diatom shell positioned over the micro-machined silicon aperture (left). The nanoporous structure of the diatom shell is seen over the aperture (right)

a) NOA 60 is a UV curable photopolymer that was applied to the boundary of the diatom where it contacts the silicon substrate. After application, the sample was exposed to ultraviolet light for 5 minutes to facilitate curing of the photopolymer.

b) Sintering process was done using high temperature treatment of the samples on which diatoms were positioned. The temperatures that were tested were 300^0 C, 400 ^{0}C and 500 ^{0}C. The sintered samples were tested for completion of immobilization by soaking in the test solution of 0.5 m KCl. In the samples heated at 400 ^{0}C and 500 ^{0}C the diatoms remained immobilized to the surface of the silicon substrate for up to 5 days in the test solution.

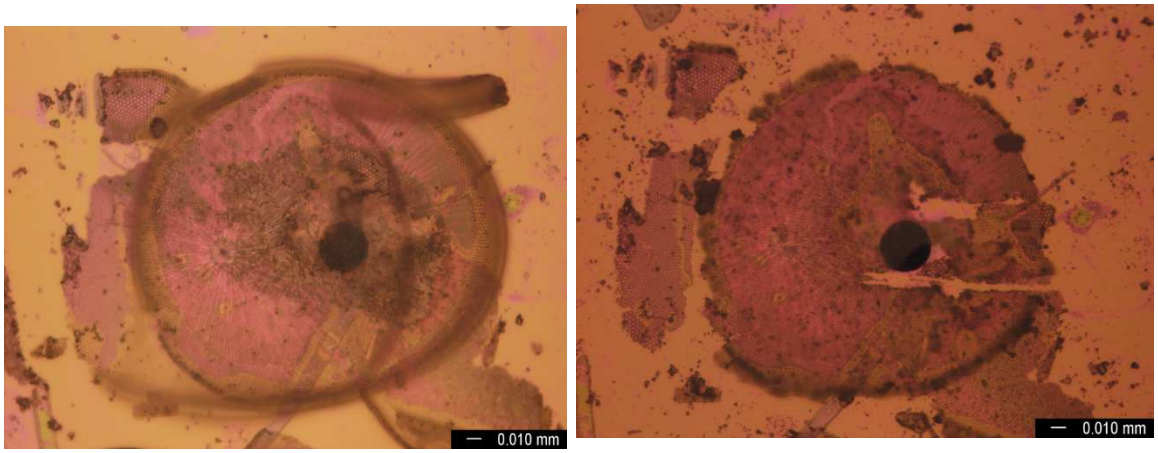

Figure 19: Diatom shells sintered at 300 ^{o}C on silicon support before (left) and after (right) soaking in a solution of 0.5 M KCl

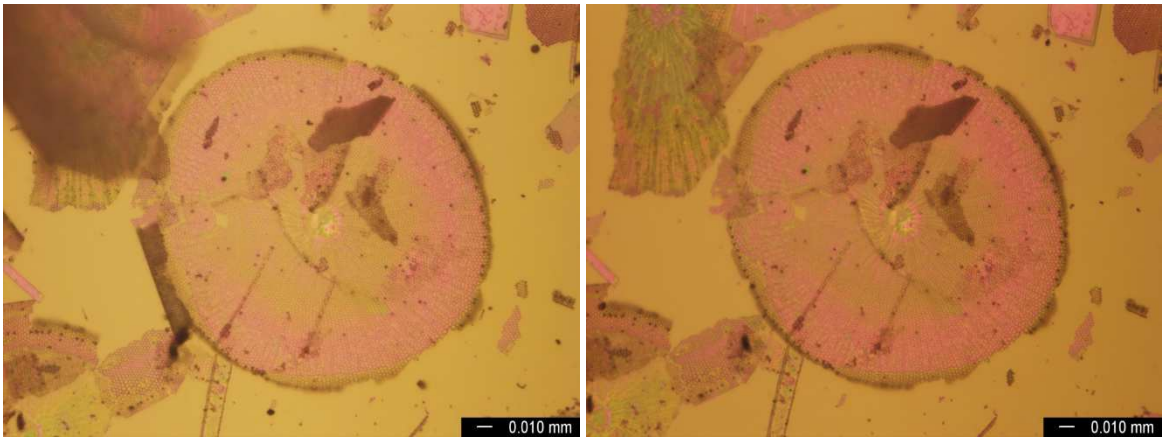

Figure 20: Diatom shells sintered at 400 ^{o}C on silicon support before (left) and after (right) soaking in a solution of 0.5 M KCl

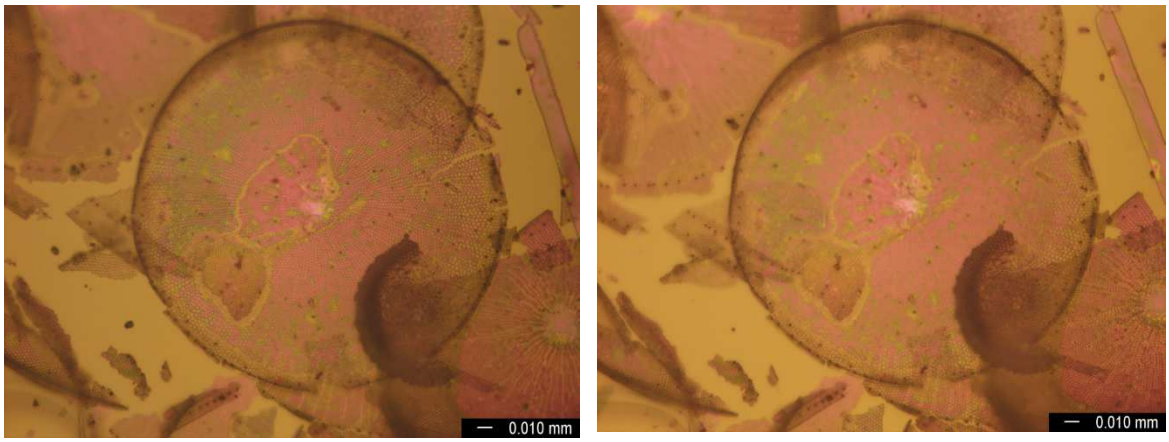

Figure 21: Diatom shells sintered at 400 ^{o}C on silicon support before (left) and after (right) soaking in a solution of 0.5 M KCl

2.5 Functionalization of Diatom – Silicon chip

The surface of the diatom shell was functionalized by two different methods: a) spin-coating it with Hexamethyl disilazane (HMDS) and b) incubating in 20 % solution of Trimethylchlorosilane (TMCS) in 1-Hexane. The spin coating of HMDS was done at a speed of 3000 rpm in atmospheric conditions. In another method, TMCS was used for functionalizing the surface by incubating the immobilized diatom in a 20% solution of TMCS in 1-Hexane for two hours, in atmospheric conditions. The sample was then washed with 1-Hexane to remove excess TMCS from the surface.

2.6 Contact Angle Measurement

In this measurement a 5µl droplet of water placed on the unmodified surface made a contact angle of 34.2 ^{0} as shown in Fig. 22 (left). After surface functionalization by spin coating with HMDS the contact angle measured was found to be 58.2 ^{0}, (Fig. 22 (center)) proving that the surface was rendered hydrophobic. A 5µl droplet of ultrapure water placed on the surface after functionalization with TMCS made a contact angle of 74.44 ^{0}. Measurements were also made on plain silicon chips that were functionalized for a week and two weeks.

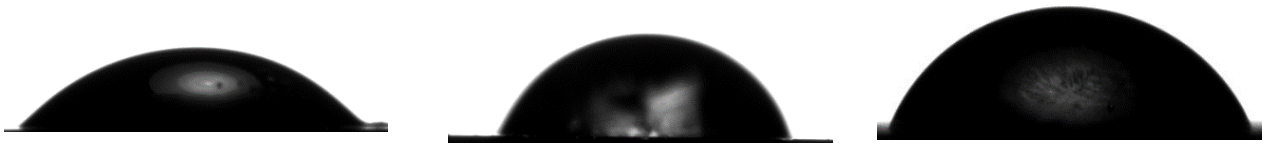

Figure 22: 5 µl droplet of ultrapure water placed on plain diatom – chip (left), diatom – chip functionalized with HMDS (center) TMCS (right)

2.7 Preparation of electrolyte solution

Potassium chloride (KCl) buffer at a concentration of 0.5 M was used for the lipid bilayer measurements for Impedance Spectroscopy and OmpF reconstitution. These were buffered with 10mM N-(2-hydroxyethyl) piperazine-N'-(2 ethanesulfonic acid) (HEPES). The molecular weight of KCl is 74.55 g/mol while that of HEPES is 238.31 g/mol. Thus, the amounts of KCl and HEPES required for preparation of 250 ml, 1.0 M KCL solution were 18.638 g and 4.766 g respectively. Since the HEPES added makes the solution acidic, the pH of the solutions needs to be increased. The final solution was titrated to a pH of 7.4 using 1.0 M potassium hydroxide (KOH) solution.

2.8 Preparation of lipid solutions

Phospholipids 1-palmitoyl-2-oleoyl-*sn*-glycero-3-phosphoethanolamine (POPE) and 1-palmitoyl-2-oleoyl-sn-glycero-3-phosphocholine (POPC) ordered from Avanti Polar Lipids, Inc. were used for ion channel reconstitution experiments. The fluorescent lipid 1, 2-dioleoyl-*sn*-glycero-3-phosphoethanolamine-N-(lissamine rhodamine B sulfonyl) (Liss Rhod PE) was used in fluorescence experiments. A 3:1 mixture of POPE and POPC in decane (10 mg/ml) was used in reconstitution experiments. A 3:1 mixture of Liss Rhod PE and POPC in decane (10 mg/ml) was used in fluorescence experiments.

2.9 Experimental Setup

The diatom-chip was sandwiched between two acrylic compartments with openings that can hold the ionic solution as shown in Fig. 23. A leak-proof seal was achieved using Viton ® fluoropolymer elastomer gaskets on both the cis and trans side of the arrangement.

Since the current signal to be measured is on the order of picoamperes, the signal-to-noise ratio has to be sufficiently large so that signal does not get lost under noise. Experimental measurements are conducted in the same frequency range as equipment power supplies and general lighting in the room. The measurements are also affected by mechanical vibrations of the system. To carry out low noise measurements, it is of utmost importance to build a measurement setup that is electrically isolated, properly grounded and mechanically stable.

These low voltage measurements are sensitive to 60 Hz noise. With no shielding, one would see periodic 60 Hz noise spikes in the output current signal; thereby distorting it. Hence, a Faraday cage was used in shielding the bilayer system from electromagnetic radiation. A metal locker which was properly grounded served as an effective Faraday cage. The noise sources include overhead lighting system in the room, computer monitors, amplifier power supplies, transformers, switch mode power supplies and any switching elements in the vicinity of the bilayer system.

Mechanical vibrations are also detrimental to measurements. Major sources of mechanical vibration include people walking near the setup, audible conversations, cooling

systems and closing of Faraday cage. An active isolation vibration table from Halcyonics was employed in removing effects of mechanical vibrations. In an active vibration control set-up, the signals acquired by extremely sensitive vibration detectors are analyzed by electronic circuitry driving electro-dynamic actuators which instantaneously produce a counter-force to compensate for the vibration. The active damping system has no resonance and no amplification of vibrations at any frequency.

A single ground point is also important to prevent noise due to ground loops between different parts of the setup. All metal equipment including the patch clamp amplifier headstage, the Autolab potentiostat used for impedance spectroscopy, the Faraday cage and the anti-vibration table should be electrically connected to a single point to prevent ground loops due to different paths to ground. A ground loop would enable a magnetic field to induce a potential difference between different points, for example, the bilayer ground and the electronics ground, resulting in a large excess noise current (Sigworth 1995)

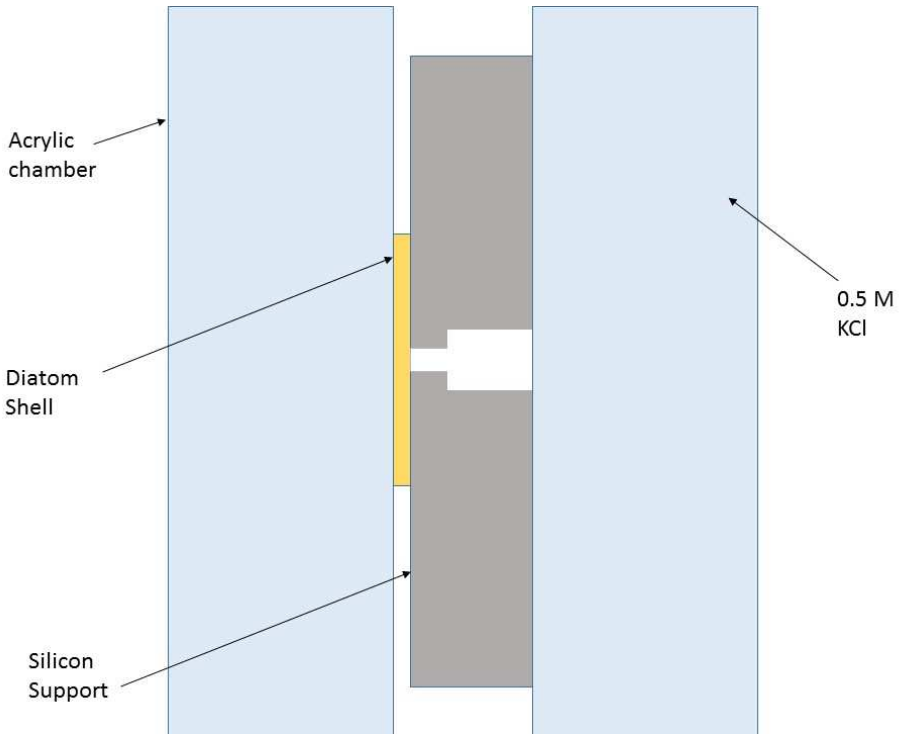

Figure 23: Experimental setup showing the diatom-chip, sandwiched between the acrylic chambers containing the ionic solution

2.10 Impedance Spectroscopy

Lipid membrane resistance and capacitance were monitored at 10 mV sinusoidal voltage with no offset over a frequency range of 0.1 Hz to 10 kHz using impedance spectroscopy. The spectroscopy was performed using Autolab PGSTAT 302 Potentiostat, with each scan lasting 11 minutes. Platinum wires were used as working and counter electrodes.

2.11 Formation of nano-BLMs and self-insertion of OmpF

In current measurement experiments, silver wires were used to make the Ag/AgCl electrodes. The Teflon insulation from the ends of silver wires was stripped and then the silver ends were inserted into common household bleach (5% NaOCl) until a thick layer of AgCl formed on the wires (usually for ~15 minutes).

AgCl forms a white colored salt that is oxidized in light and changes to a black color. It is important that the ends of the wires are completely chloridized or covered with the Teflon insulation so that no bare silver is in contact with solution otherwise electrode potential would drift (Sakmann 1995).

Around 1 µl solution of lipid mixture consisting of 10 mg/ml POPE and 10 mg/ml POPC in the ratio 3:1 in hexane was applied to the surface of the nanoporous membrane. After impedance analysis of the formed bilayer, around 1 µl of OmpF solution was added to the cis-side of the arrangement.

CHAPTER 3

RESULTS

3.1 Simulation

The simulated current pulse is presented in Fig. 24 as a function of position of the polystyrene sphere along the length of the aperture.

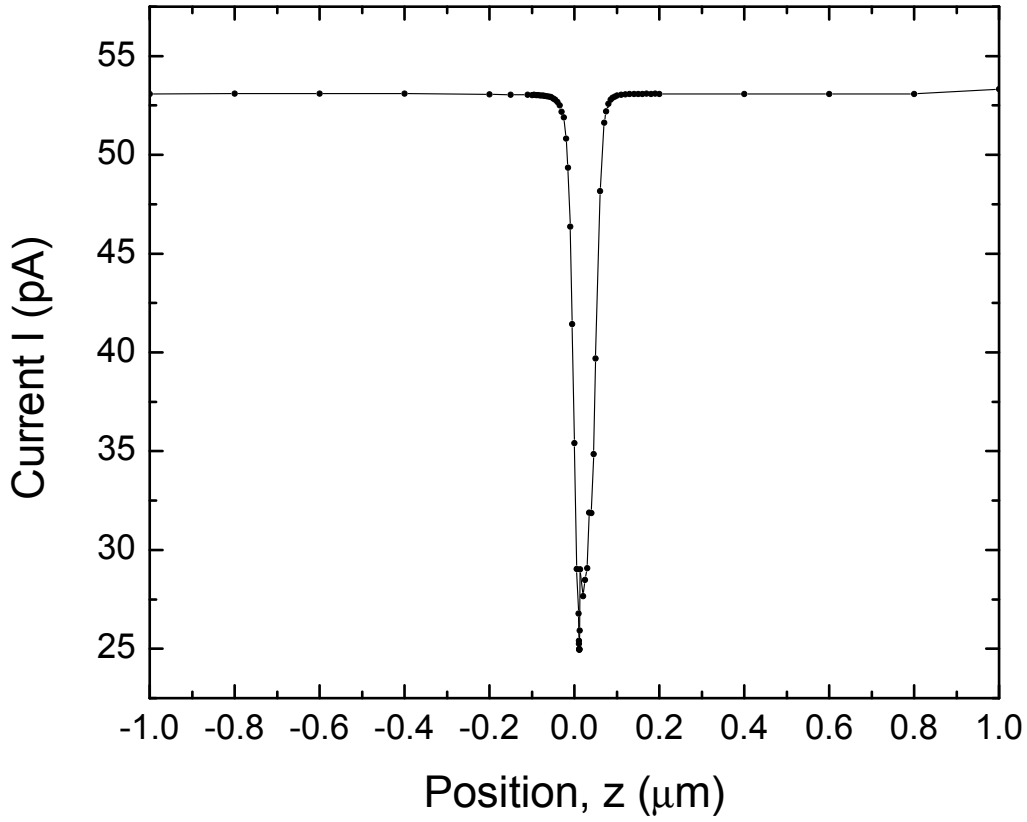

Figure 24: Simulated current when a 27 nm polystyrene bead translocates through a diatom – chip

The maximum current reduction obtained from the simulation was 28.36 pA. The accuracy of this simulation was tested by comparison of the maximum reduction in current predicted by theory as follows.

The theoretical reduction in current during the translocation events of 27 nm polystyrene spheres through a 40 nm aperture of length 50 nm can be described by the theory of Coulter counting. To account for the crowding of the electric field lines around the nanoparticle inside the aperture, DeBlois and Bean introduced a correction factor S in the current drop relationship as follows:

$$\Delta I = I_0 S(d/D)\frac{d^3}{l \cdot D^2} \quad \ldots (18)$$

where, ΔI is the current drop, I0 is the base line current in the empty aperture, d is the nanoparticle diameter, D is the aperture diameter, and l is the length of the cylindrical aperture. When the diameter of the translocating nanoparticle (d) approaches the diameter of the aperture (D), current crowding or electric field bulging occurs, which causes a non-linearity in the relationship between the particle size and the current reduction pulse. The non-linearity is included in the expression by the empirical factor S (d/D), given by

$$S\left(\frac{d}{D}\right) = [1 - 0.8\ \left(\frac{d}{D}\right)^3]^{-1} \ldots (19)$$

In the case of small particles in large apertures, when d/D < 0.5, the value of S is negligible (S (0.5) = 1.110694). However, as d/D increases above 0.5, S is necessary in order to prevent the over-estimation of the nanoparticle size due to current crowding. In the case of a 27 nm nanoparticle and 40 nm aperture (d/D = 0.675), the value of S is calculated as 1.3263.Under the assumption that the current flow is limited by the smallest aperture of 40

nm and a length of 50 nm, the baseline current for cylindrical aperture geometry is given by:

$$I_0 = V \cdot \frac{\pi \cdot \sigma \cdot D^2}{4 \cdot (l + 0.8D)} \quad \ldots (20)$$

Using Nernst-Einstein relationship, $\sigma = \frac{\sum_i c_i D_i z_i^2 F^2}{RT}$, to obtain the conductivity for 1 mM KCl of 149.8 μS/cm and (20) to determine a baseline current of 91.7 pA at 400mV, the theoretical current reduction estimated by (18) is found to be 29.95 pA. The simulated reduction in current (28.36 pA) deviates by 5% from the theoretical value.

The translocation events of 27 nm polystyrene spheres through the diatom-chip, visible in the form of ten distinct pulses within 120 seconds, resulted in an average current reduction of 28.69 ± 4.12 pA. The differences in current amplitude for these single translocation events can be attributed to two sources (i) the small non-uniformity of the aperture size distribution and (ii) the size distribution of the polystyrene spheres (27 nm ± 2.7 nm). The accuracy of the simulation is thus substantiated by close correspondence with experimental result as illustrated in Fig. 25.

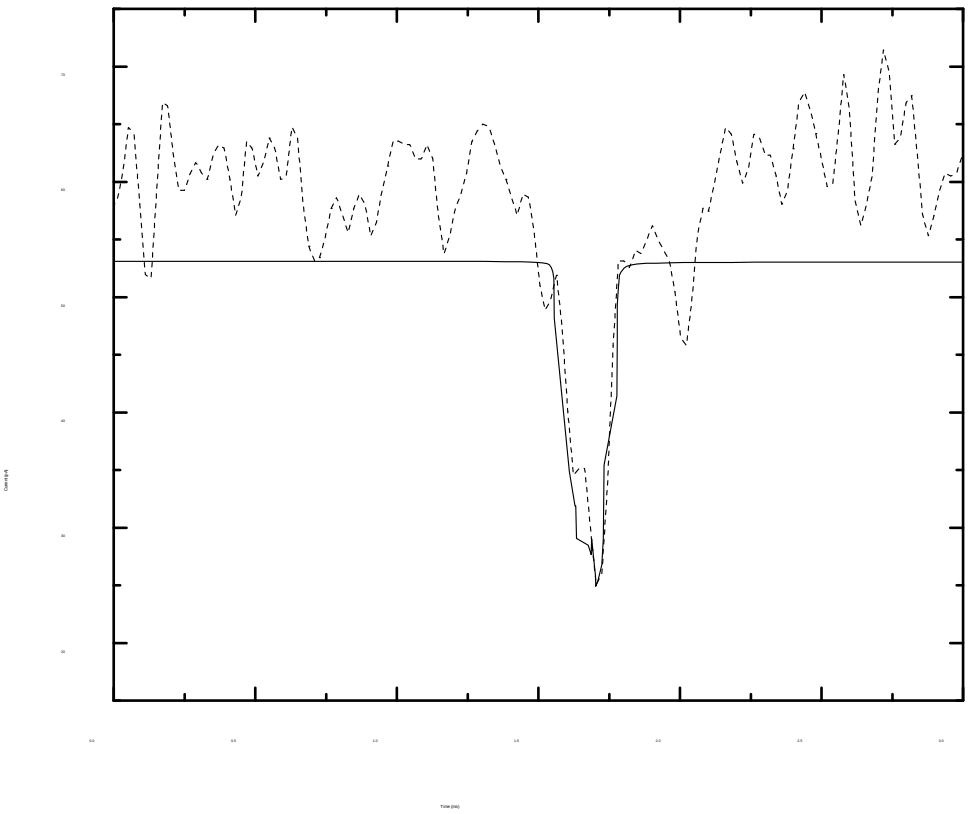

Figure 25: Measured current when a 27 nm polystyrene bead translocates through a 40 nm wide, 50 nm long pore

The translocation time is defined as the width at 50% of the current reduction pulse height. From the experimental results, the average translocation time was 155 ± 90 μs. Again, the high standard deviation stems from size distributions of apertures and polystyrene spheres, as well as limitation from the time resolution of 20 μs in measuring the experimental current. The average experimental translocation time (155 μs) was then used to convert the simulated current from position-dependence to time dependence using

an assumed value for the mobility (μ_p) of the polystyrene sphere. Note, the value of the mobility did not affect the magnitude of simulated current reductions.

The position-dependent velocity of the particle, v_p was calculated using μ_p . E, where E is the position-dependent electric field in the direction of motion. An assumed value for μp of 1.11 x 10^{-8} $m^2s^{-1}V^{-1}$ yields a translocation time of 159.45 μs, which is within 2.8 % of the average experimental value. Although ζ – potential measurements are needed to accurately determine the mobility of 27 nm polystyrene spheres, the literature value for 80 nm polystyrene spheres (2.8 x 10^{-8} $m^2s^{-1}V^{-1}$) indicates that the assumed value is in an acceptable order of magnitude (White, et al. 2007).

In order to demonstrate the validity of the simulation, the maximum current reduction values for polystyrene beads in 1 mM KCl were simulated as a function of the dimensionless diameter ratio (d/D), with d being the particle and D the nanopore diameter. The simulation was based on a nanopore of diameter D of 40 nm and a length l of 50 nm.

The simulation results were compared to the values obtained from the analytical expression for the current reduction from (18) and are shown in Fig. 26. From the results it can be inferred that the simulated maximum current reduction values and the values obtained using the analytical expression (18) are starting to deviate for diameter ratios d/D > 0.4. This divergence for d/D > 0.5 is expected due to the influence of the nanopore geometry on the current crowding factor S (d/D) in (18).

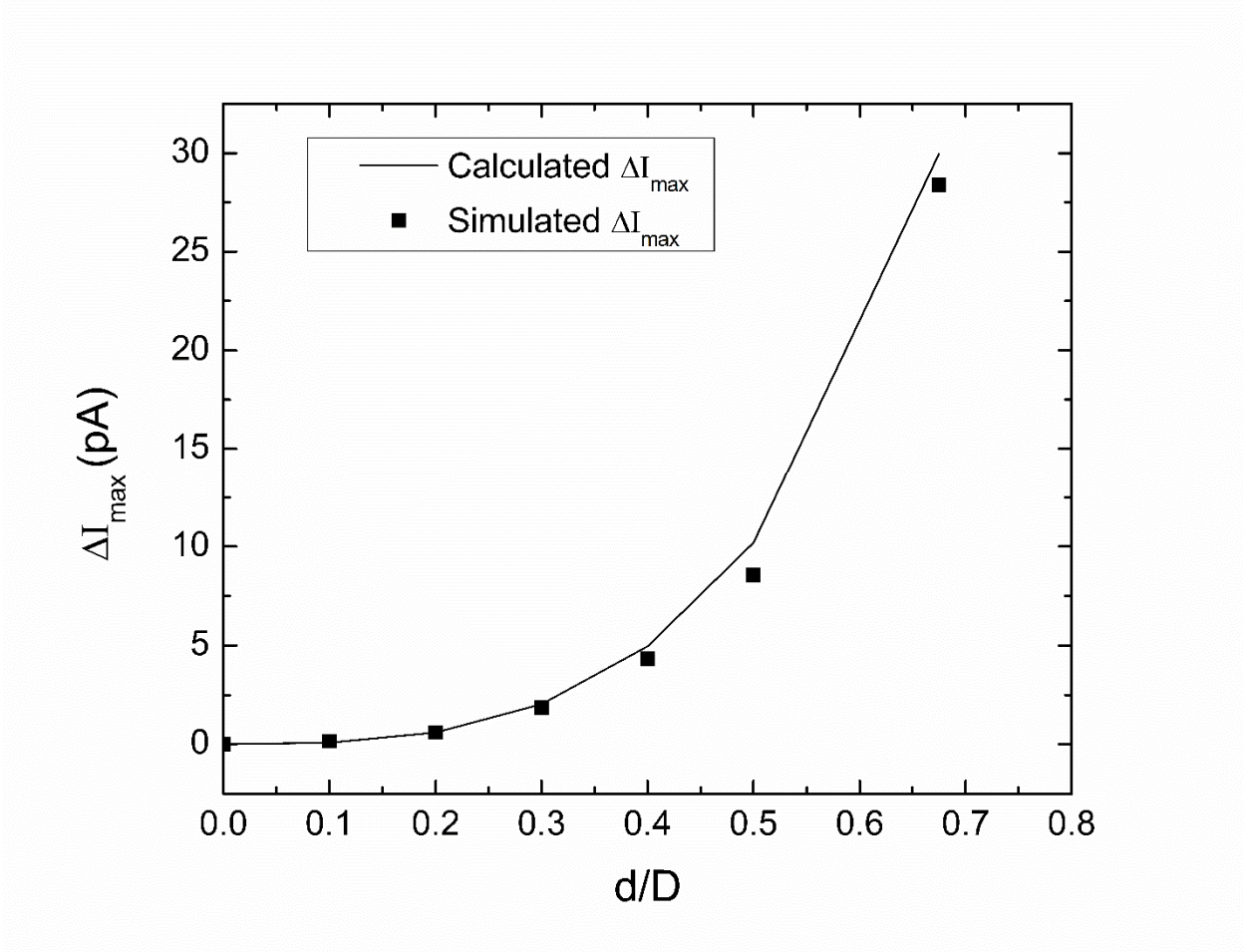

Figure 26: Comparison between maximum current reduction values (ΔI_{max}) obtained via numerical simulation (squares) and an analytic expression (solid line) for different diameters of polystyrene spheres (d) translocating through an aperture of diameter D of 40 nm and length l of 50 nm.

3.2 Surface Functionalization

The goal of the project was to investigate the feasibility of forming free-standing bilayer lipid membranes across the 40 nm - 60 nm diameter nanopores of the immobilized diatom shell. Initial experiments in trying to form pore-spanning nano-Lipid bilayer membranes were successful only 1 out of 10 times. The low formation probability of the lipid bilayer

membranes can be attributed to the hydrophilic nature of the cleaned diatom shells. As discussed in Section 1.1.4, it has been reported that lipid bilayers span the nanoporous apertures when they are functionalized to be hydrophobic in nature. Contrary to that, lipid bilayers have been found to line the inner surface of on-functionalized hydrophilic glass nanopores. Based on the low initial lipid bilayer membrane formation probability due to the hydrophilic nature of the biogenic nanopore membranes, a surface functionalization was performed as discussed in Section 2.5 and the success and resulting hydrophobicity of the surface was verified by two tests: i) Fourier Transform Infrared Spectroscopy (FTIR) measurements and ii) Contact angle measurements of ultrapure water on the functionalized surface.

3.2.1 Fourier Transform Infrared Spectroscopy

The FTIR characterization of plain oxidized silicon and surface-modified silicon substrates was carried out in the range of 400–4000 cm^{-1} at a resolution of 4 cm^{-1} with an average over 128 scans to obtain information about surface bonding characteristics and evidence of surface modification. The intensity was measured on a Spectra-Tech infrared microscope with a 15x Cassegrain objective in reflectance mode, using a liquid nitrogen cooled Mercury Cadmium Telluride (MCT) detector.

The intensity of the infrared light reflected from a oxidized silicon chip (ISi) that was cleaned using a piranha solution (Sulfuric acid and Hydrogen Peroxide) was used as the reference. Then the intensity light reflected from a silicon chip functionalized with TMCS for two weeks (I_{TMCS}) was recorded subsequently. The relative intensity of light reflected from the functionalized diatom-chip to the reference chip was found using

$$\text{Relative intensity of light} = \log_{10} (I_{Si} / I_{TMCS})$$

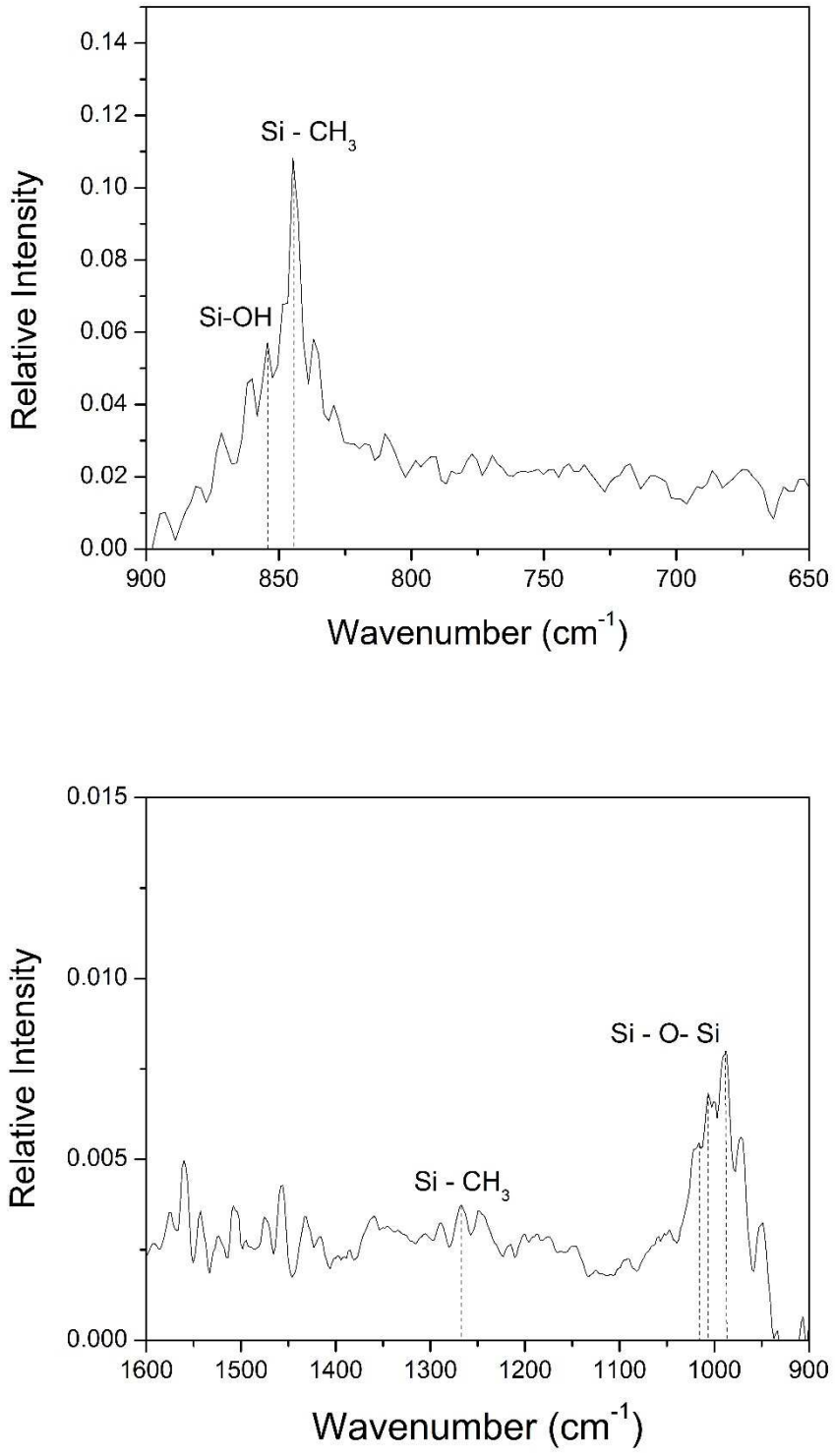

Figure 27: Relative intensity of light reflected by Silicon chip modified by TMCS with a plain Silicon chip as reference.

Wavenumber (cm^{-1})	Range (cm^{-1})	Identification
844	840-750	$Si\text{-}CH_3$
1269	1275-1245	$Si\text{-}CH_3$
854	910-850	Si – OH
1006	1130-1000	Si – O – Si

Table 2: Infrared spectra, peak identification (Anderson 1993) (Launer 1987)

The relative intensity between light reflected from a plain silicon chip and surface-modified silicon chip is shown in Fig. 27. The peaks between 1000 and 1050 cm^{-1} are identified as vibration modes of Si–O–Si, which confirms the formation of a Si–O–Si network on the chip surface. The peak at 1269 cm^{-1}, corresponds to the symmetric deformation vibration of C–H bonds, representing the attachment of methyl group with Si. Table 3 shows the identification of the chemical bonds present on the surface modified chip with their corresponding wavenumbers. The relatively smaller Si–OH peak at 854 cm^{-1} compared to the peak at 844 cm^{-1} that is associated with the rocking vibration of the Si–C bonds shows the removal of –OH group and the creation of Si – C bonds. The presence of carbon groups on in the functionalized surface in the range 650–900 cm^{-1} indicates the formation of hydrophobic surface termination of the chip. As a result of the FTIR measurement it can be inferred that after TMCS surface treatment, some of the hydroxyl groups get replaced by methyl groups, which changes the hydrophilic nature of to the chip surface to hydrophobic. In order to quantify the hydrophobic nature of the chips using work of

adhesion and to find the optimum amount of functionalization time needed to successfully span lipid bilayers across the nanoporous membranes, contact angle measurements were carried out on silicon chips functionalized for increasing periods of time.

3.2.2 Contact Angle Measurement

The results of the contact angle measurement from Section 2.8 were used to assess the hydrophobic nature of functionalized and also to estimate surface free energy. The low contact angle of 34.2 ^{0} on the plain unfunctionalized chip shows that the surface of the chip is hydrophilic due to the presence of silanol (Si–OH) groups. After the surface modification with TMCS for 2 hours, the contact angle of the Silicon chip surface increased to 74.44^0. The increased water contact angle indicates the replacement of some of the – OH groups on the surface by hydrophobic groups. The contact angle measurement was repeated for the silicon chips functionalized for a week and two weeks to increase the number of replaced – OH groups on the surface. The surface free energy and work of adhesion was calculated for each case to quantify the result.

The surface free energy and the work of adhesion can be calculated using the Neumann's equation of state and the Young's equation (Mahadik 2011) . The static contact angle is given by Young's equation

$$\gamma_{lv} \cos\theta = \gamma_{sv} - \gamma_{sl} \quad \ldots (21)$$

The Neumann's equation of state is given by,

$$\gamma_{sl} = \gamma_{lv} + \gamma_{sv} - 2\sqrt{\gamma_{lv}\gamma_{sv}}e^{-0.000125(\gamma_{lv} - \gamma_{sv})^2} \quad \ldots (22)$$

Where, θ is the contact angle, γlv is the interfacial surface tension of liquid vapour interface, γsl is the interfacial tension of solid liquid interface, and γsv is the apparent surface free energy of the solid. Combining (21) and (22) yields,

$$\cos\theta = -1 + 2\sqrt{\frac{\gamma_{sv}}{\gamma_{lv}}}e^{-0.000125(\gamma_{lv} - \gamma_{sv})^2} \ldots (23)$$

Γsv can be calculated based on known values of γlv and θ. The work of adhesion is then defined as

$$W_a = \gamma_{sv} + \gamma_{lv} - \gamma_{ls} \ldots (24)$$

For the silica chips modified with TMCS, the apparent contact angle, θ, measured for water was found to be increased from 34.2 to 92.1 with an increase in silylating time from two hours to two weeks (Table 2). The increase in contact angle indicates the increase in hydrophobicity of the surface of the silica chip which is due to replacement of some of the polar –OH groups on the surface by non-polar $–CH_3$ groups due to silylation. These results correspond to the results obtained from FTIR spectroscopy performed on the chip that has been functionalized for two weeks.

The surface free energy of a solid determines its surface and interfacial behavior in processes like wetting and adhesion. For apparent surface free energy calculation, the surface tension of water, γ_{lv}, was taken as 71.99 mN/m, while the observed contact angle θ was taken in degrees. The γ_{sl} and γ_{sv} were calculated using (22) and (23), respectively. The calculated values for γ_{sl} and γ_{sv} and work of adhesion (Wa) for the TMCS functionalized silicon chips are presented in Table 3. The contact angle θ was found to increase from 74.44

to 92.1 resulting in decrease in apparent surface energy, γ_{sv}, from 38.37 to 27.404 mJ/m^2 and increase in interfacial tension between solid-liquid interface, γ_{sl} from 19.095 to 30.106 mN/m. The apparent surface free energy calculations revealed that with increase in silylating time at room temperature the wettability of the surface of the silicon chip decreased. These results are also supported from the work of adhesion calculations. The work of adhesion, Wa, decreased from 19.671 to 6.257 mJ/m^2.

To check the effect of functionalizing the surface on the aperture conductivity in solution, the functionalized chips were placed in the experimental setup and tested for electrical conductivity. It was observed that the apertures in the diatom frustules that were functionalized for one week and two weeks did not fill with the electrolyte. This indicates that although increased silyation time resulted in a better hydrophobic coverage of the silicon chip surface as indicated by the increased contact angle and surface energy, the amount of hydrophobic functionalization also determines if the apertures on the silica shell allow the entry of the electrolyte into them, which is critical when attempting to perform electrophysiology measurements. It can be inferred from these results that the apertures of the diatom shell need to be functionalized to become hydrophobic in a limited range of surface energy (~ 38 – 31 mJ/m^2) so that it allows the electrolyte to fill the apertures and establish conductivity between both sides of the nanoporous membrane before a lipid bilayer membrane will be formed across the apertures.

Functionalization Time	Conducting apertures filled with electrolyte	Contact Angle (degrees)	Surface Tension γ_{sl} mN/m	Surface Energy γ_{sv} mJ/m^2	Work of adhesion W_a mJ/m^2
Unfunctionalized	Yes	34.2	2.155	61.67	131.521
2 hours	Yes	74.44	19.095	38.370	91.270
1 week	No	85.8	26.085	31.315	77.219
2 weeks	No	92.1	30.106	27.404	69.288

Table 3: Effect of functionalization time on hydrophobicity of silicon chips

3.3 Impedance Spectroscopy of nano-BLMs

The impedance analysis of the functionalized sample without addition of lipids reveals that the surface functionalization of the sample did not change its electrical behavior (Fig 28). The ohmic resistance of the electrolyte through the pores was measured, thereby proving that the surface modification process adopted does not prevent the pores from being filled with the electrolyte. This result reinforces the fact that only the painted surface of the nanoporous membrane was rendered hydrophobic, whereas the pores were filled with the electrolyte to establish electrical continuity between the cis and trans sides of the holder. It also establishes that a hydrophobic surface is enough to form a stable lipid bilayer on the nanoporous membrane.

In Fig. 30, the impedance spectrum of diatom shells functionalized with HMDS after application of lipids are shown. Comparing the spectra before and after application of

lipids shows that a layer consisting of lipids has been formed across the nanoporous membrane. The formation probability of non-functionalized pores was about 1 out of 10.

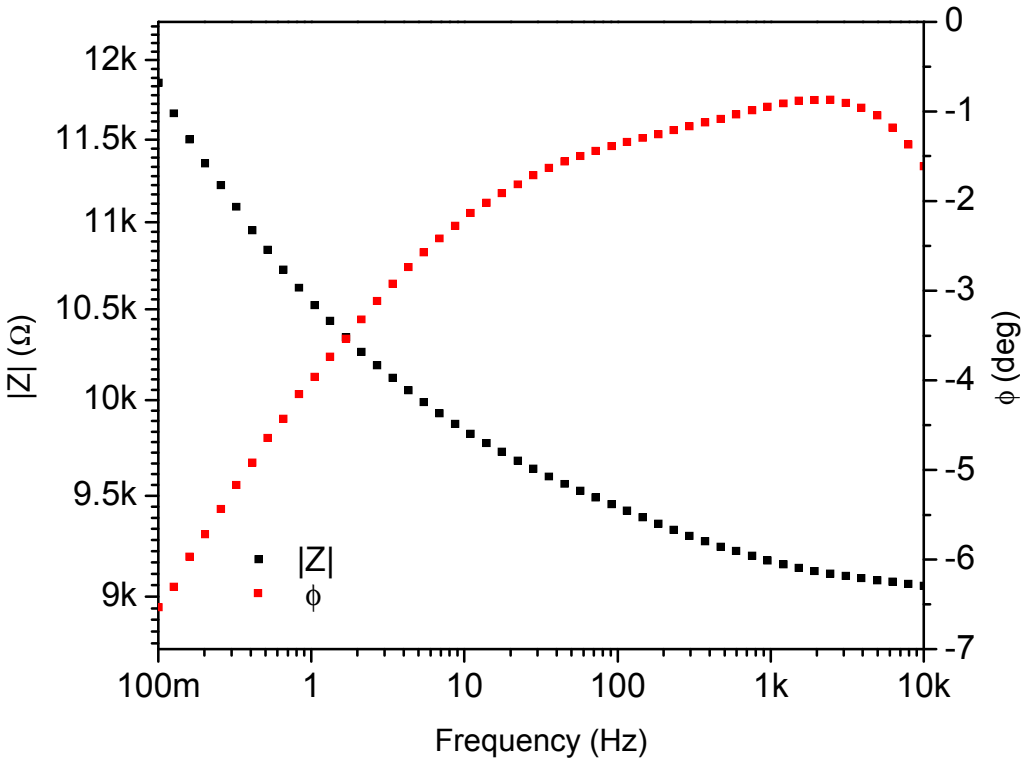

Figure 28: Impedance Spectrum of a diatom – chip functionalized with HMDS

With functionalized pores a lipid layer was formed across the pores 10 out of 10 times using both HMDS and TMCS.

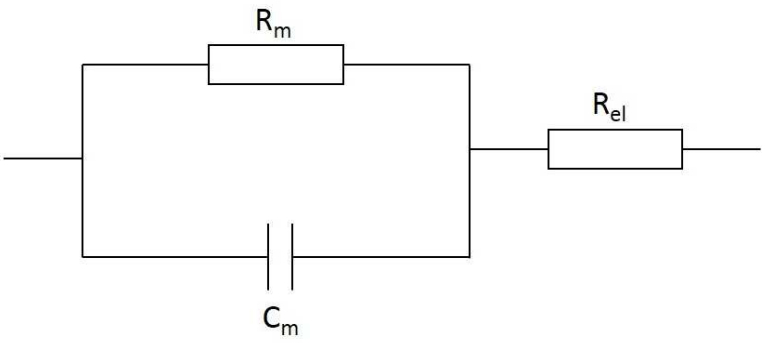

Figure 29: Equivalent circuit of a lipid bilayer membrane

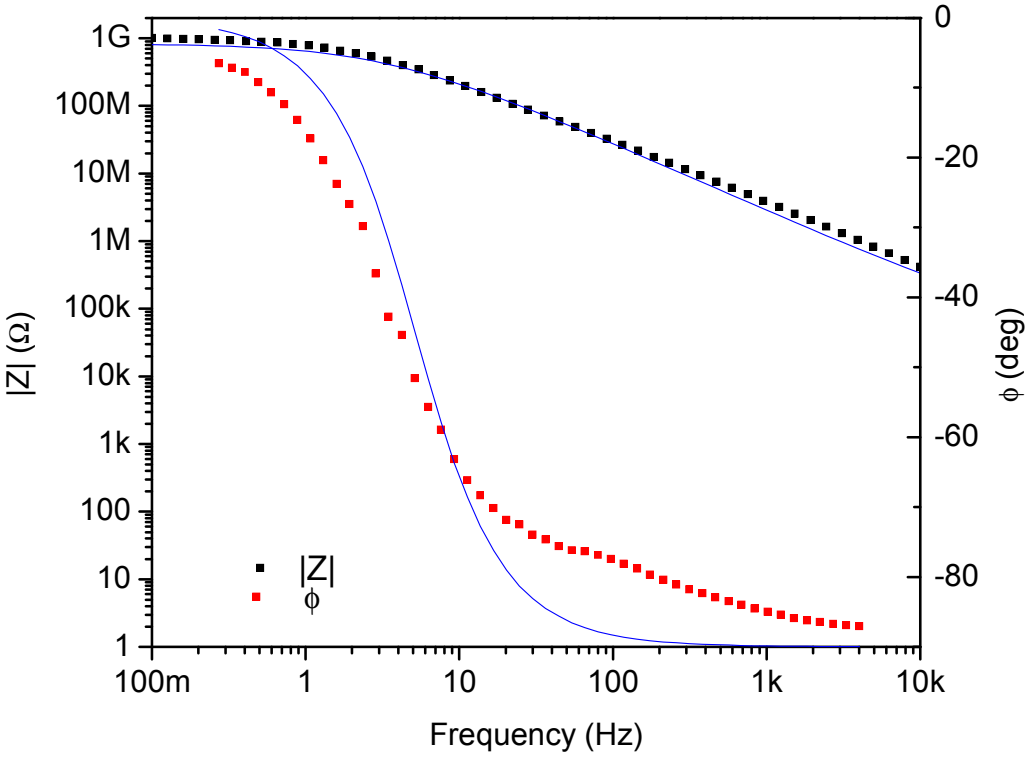

Figure 30: Impedance Spectrum of nano – Bilayer Lipid Membranes (nano – BLMs) formed across a diatom-chip functionalized with HMDS

The impedance data was used to extract membrane parameters, represented in the equivalent circuit shown in Fig. 29. The circuit consists of a parallel RC loop representing the electrical behavior of the lipid bilayer. These parameters therefore represent the membrane resistance R_m and membrane capacitance C_m of the bilayer. A resistance R_{el} is added in series to this loop which represents the ohmic resistance of the electrolyte. The electrolyte resistance is predominant in the high frequency regime above 10^4 Hz. In the range of ~ 10 to 10^4 Hz the membrane capacitance dominates the impedance spectrum which is seen by the phase angle of -90^0. At frequencies lower than 10 Hz, a gradual increase in the absolute value of phase and impedance is seen. This behavior is due to the predominance of the membrane resistance R_m in this regime. Fitting the parameters of the equivalent circuit to the data shown in Fig. 30 yields the parameters, Cm – 56.2 pF and Rm – 0.832 GΩ. The fit error for Cm was 4.47 % and that for Rm was 6.34%. The fitting error for the membrane resistance depended on its absolute value (Romer and Steinem, Impedance analysis and single-channel recordings on nano-black lipid membranes based on porous alumina 2004) leading to up to 17 % fit error. The membrane resistance measured over 20 trials ranged from 0.259 GΩ to 0.832 GΩ.

The initial formation of the lipids across the pores functionalized with HMDS was thick, indicated by capacitance values ranging from 29 pF to 35 pF. About 10 – 30 minutes after the formation, the nano - BLMs thinned down to a bilayer membrane with capacitance values greater than 50 pF.

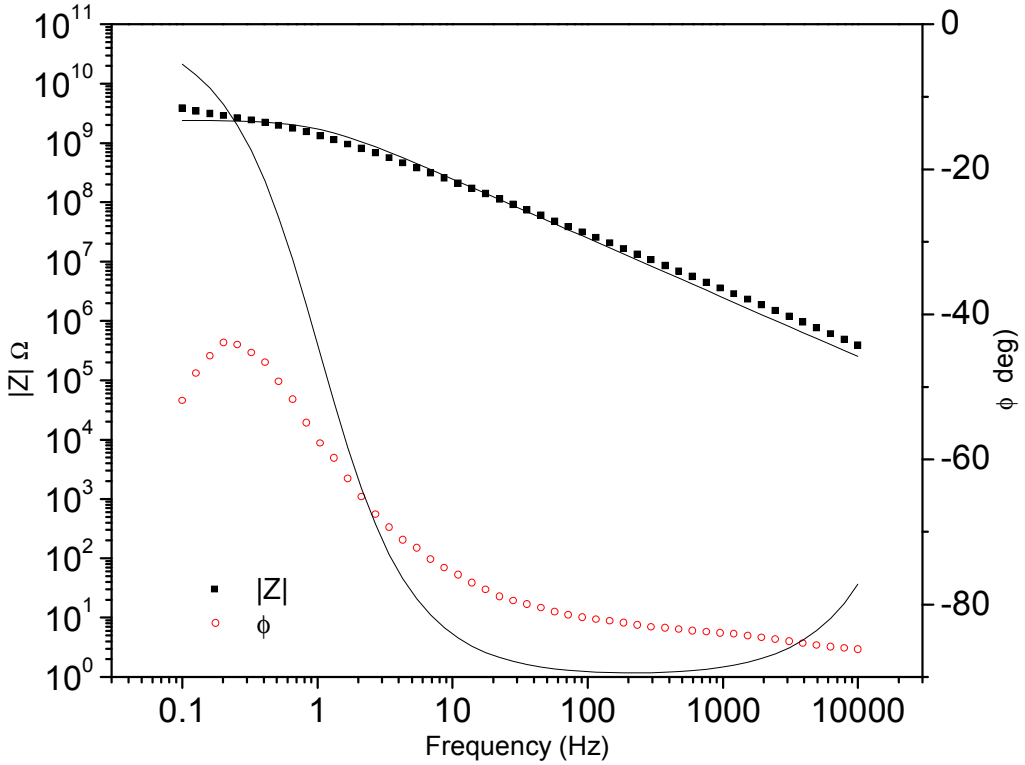

Figure 31: Impedance Spectrum of nano – Bilayer Lipid Membranes (nano – BLMs) formed across a diatom-chip functionalized with TMCS

In the case of pores functionalized with TMCS, initial bilayer formations always resulted in a Gigaseal ($R_m > 1$ GΩ). The impedance spectrum of nano-BLMs formed across diatomic shells functionalized with TMCS is shown in Fig. 30. The membrane resistance in the lower frequency range is predominant with a fit value of 2.403 GΩ and a fit error of 10.85 %. The membrane capacitance was fit in this case to be 64.1 pF with a fit error of 5.91 %. In this particular trial, the phase angle decreased from around -40^0 to -50^0 at about 0.2 Hz indicating that the resistive regime will occur at a frequency lower than the usually observed 10 Hz range.

The lifetime of Gigaseals formed varied from trial to trial. To obtain the time variation in membrane parameters after initial formation, the membrane resistance, R_m and membrane capacitance C_m were measured over a course of 4 hours using impedance spectroscopy (Fig .32).

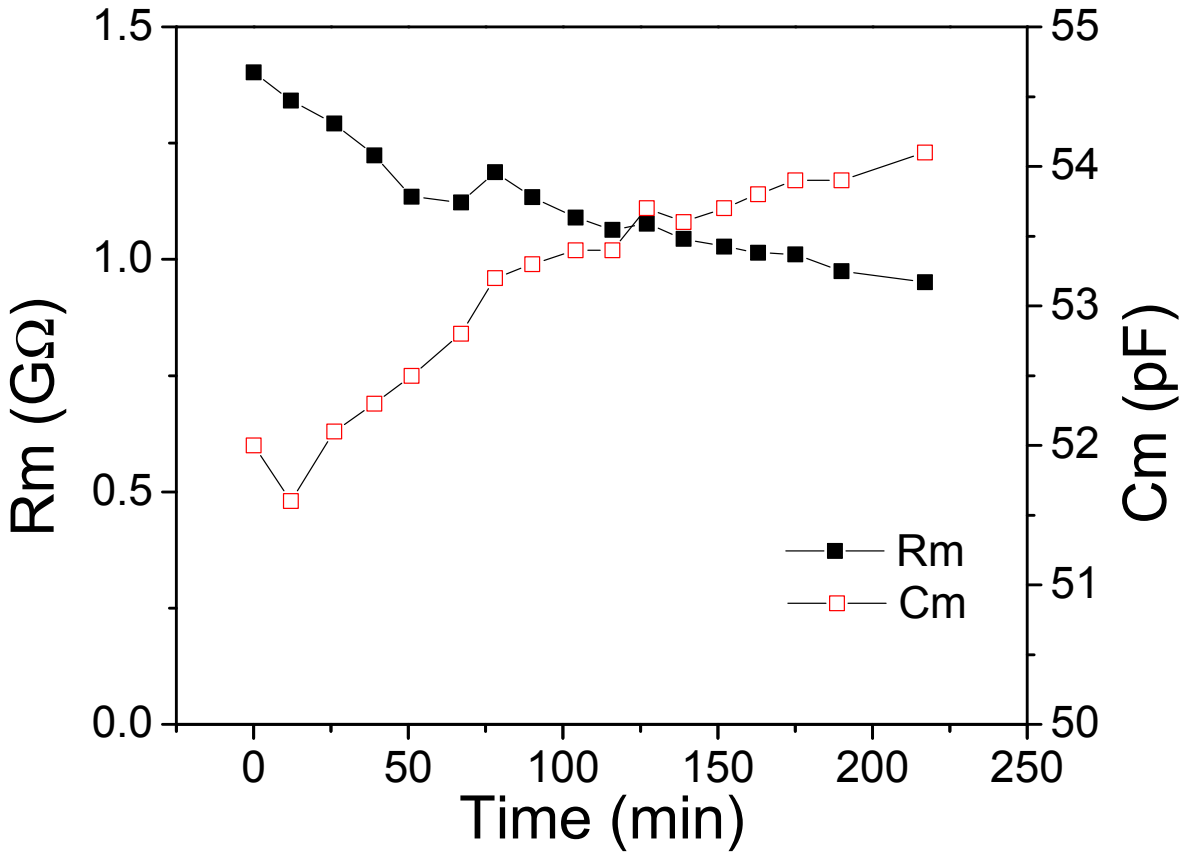

Figure 32: Time dependence of membrane resistance and membrane capacitance of nano BLMs formed across a diatom-chip functionalized using HMDS

An initial membrane resistance of 1.342 GΩ was fitted with the corresponding membrane capacitance being 51.6 pF using the equivalent circuit. The fitting error in this case was 5.475 % and 3.65 % for the resistance and capacitance respectively. The membrane resistance steadily dropped and reduced below 1 GΩ after about 3 hours for this particular nano-BLM. The membrane capacitance decreased in the initial 10 – 12 minutes and then started increasing. The fitting error increased to 6.172 % and 4.248 % for the resistance and capacitance respectively. The highest recorded lifetime of ~ 15 hours was obtained for the nano- BLM with impedance spectrum shown in Fig. 33.

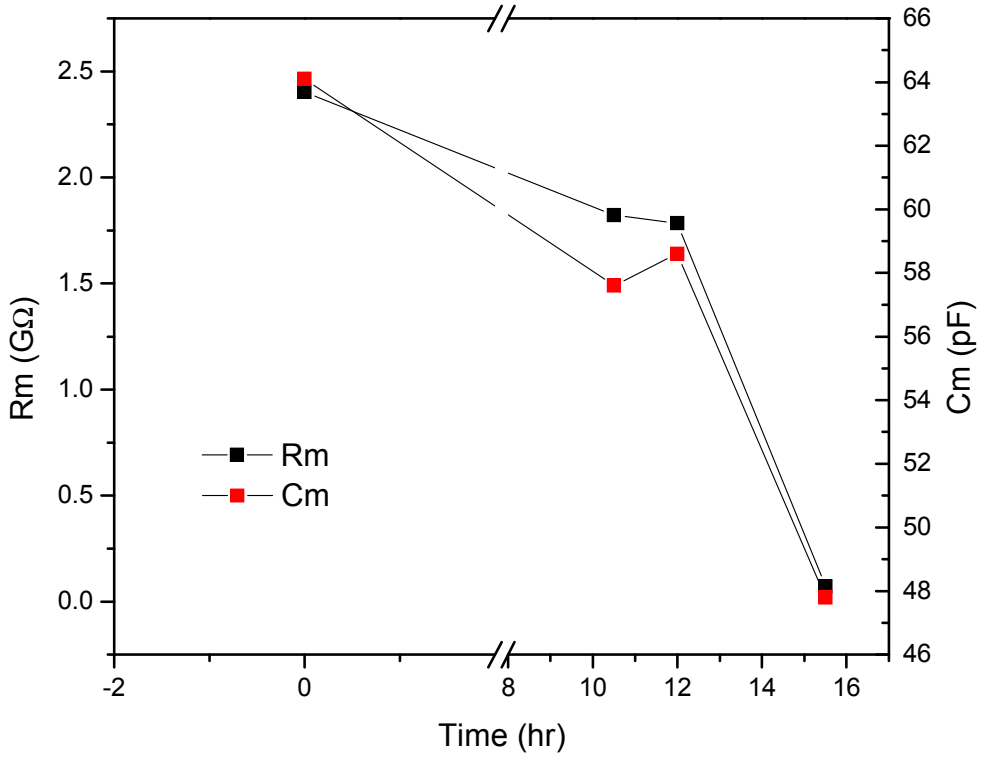

Figure 33: Time dependence of membrane resistance and membrane capacitance of nano BLMs formed across a diatom-chip functionalized using TMCS

The current vs time characteristic of the nano- BLMs recorded for different applied voltages is shown in Fig. 34. Voltages from 300 mV to 600 mV was applied in steps in 30 seconds. The current showed an increase for each voltage indicating that not all nanopores were covered with nano-BLMs. For a given voltage, the current exhibited smaller steps or bursts indicating that a lipid membrane exists and is being deformed by the electric field that exists.

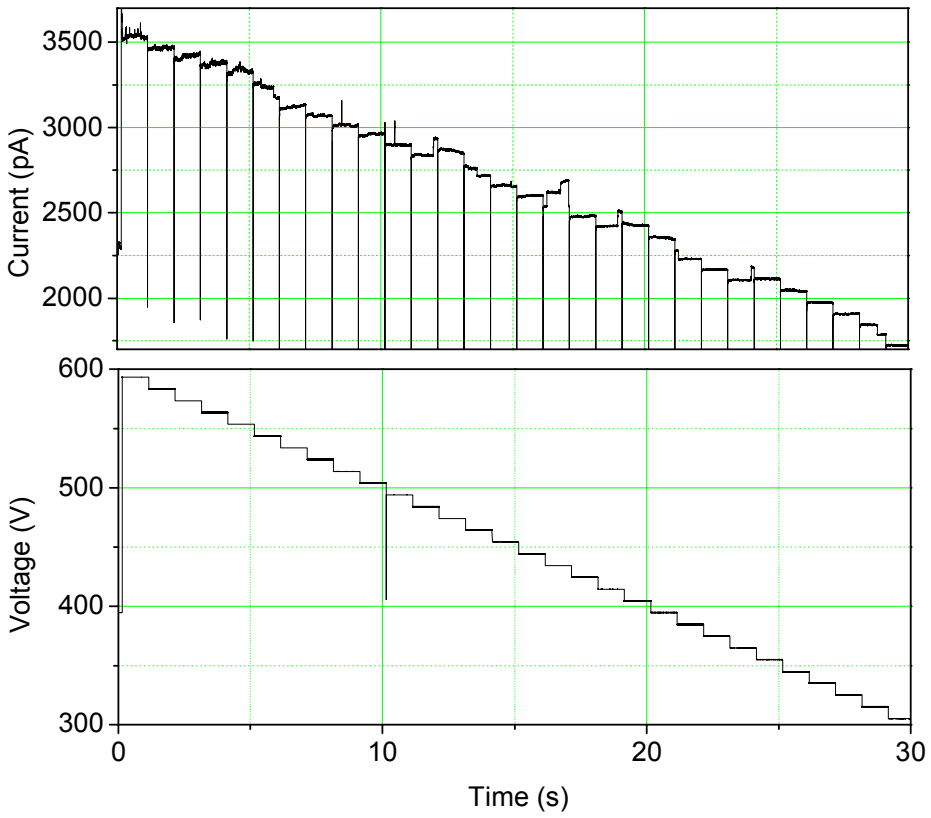

Figure 34: Current vs time characteristic of nano – BLMs for voltages in the range 300 – 600 mV

3.4 Investigation of nano – BLM structures on the diatom shell

It has been established from the time characteristic of the membrane resistance that several nano-BLMs are formed in parallel across the nanoporous diatom shell. This was concluded from the gradually decreasing value of membrane resistance over time as opposed to a

sudden rupture of a single lipid bilayer membrane. To further prove this point, an optical proof of the arrangement of the nano-BLMs across the nanoporous diatom shell was required. This was achieved by painting the nanoporous surface with phospholipids that are headgroup labeled with a fluorescent compound. The fluorescent lipid 1,2-dioleoyl-*sn*-glycero-3-phosphoethanolamine-N-(lissamine rhodamine B sulfonyl) was ordered from Avanti Polar lipids for this purpose. Nano – BLMs were formed across the diatom – chip substrate and were imaged to optically prove the parallel arrangement of individual nano-BLMs.

Using lipids tagged with Rhodamine B gave an insight into the spanned structure of lipid bilayer membranes in non-functionalized diatom-chips and functionalized chips as seen in the images obtained in Fig. 35 and Fig 36.

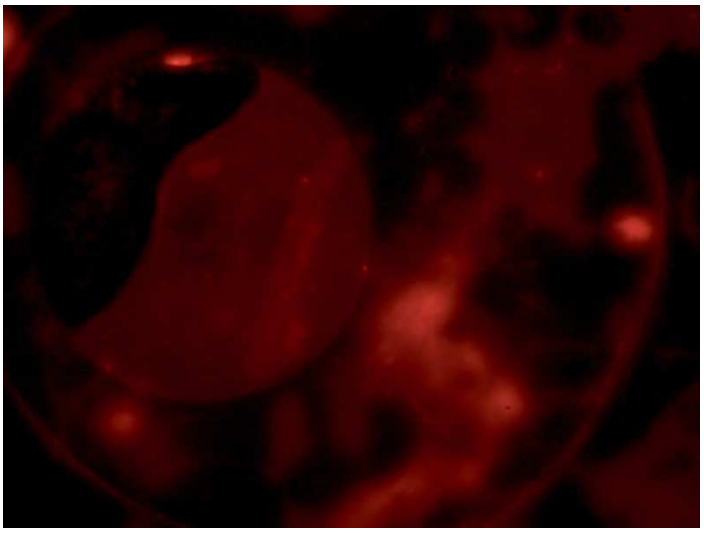

Figure 35: Fluorescence image of non-functionalized diatom-chip

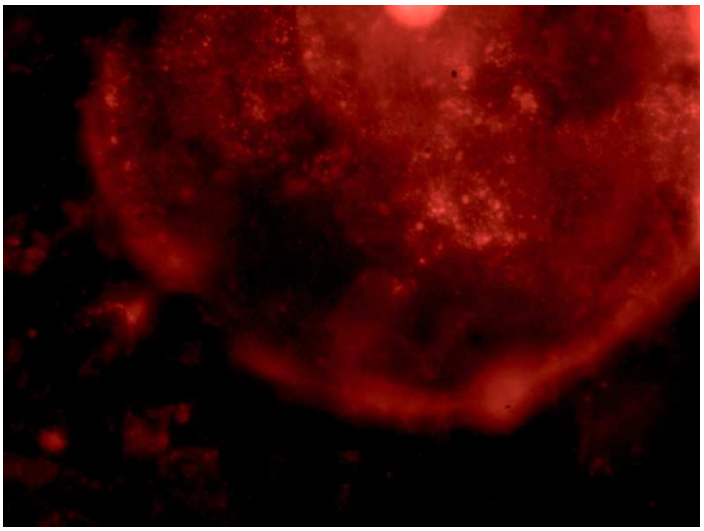

Figure 36(a): Fluorescence image of diatom-chip functionalized with TMCS

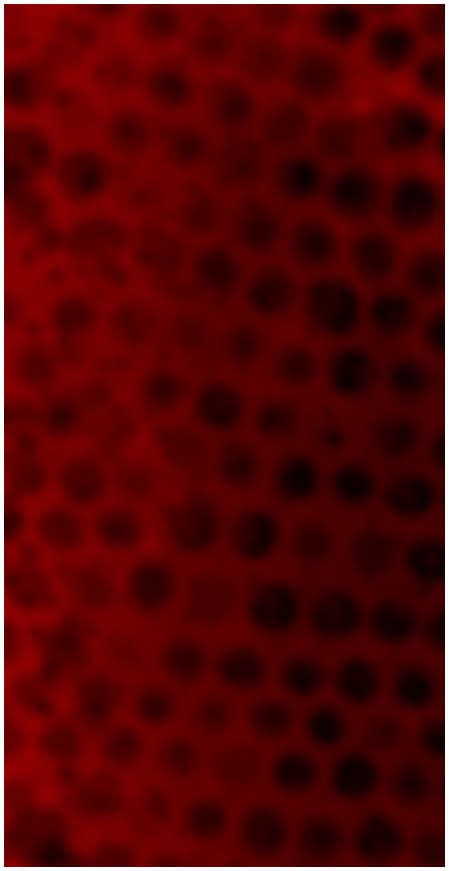

Figure 36 (b): Fluorescence image taken using a Leica SP2 Confocal microscope using a water immersion lens showing pores spanning lipid bilayers on the left hand side.

3.5 OmpF reconstitution in nano-BLMs

The nano-BLMs that could be formed across the biogenic substrates functionalized with TMCS are suited for single-channel recordings as they exhibit membrane resistances > 1GΩ. The outer membrane protein OmpF of E. Coli was chosen for recording transmembrane ionic currents. Reconstitution into the formed bilayers was done by introducing the protein solution in detergent to the cis compartment of the experimental setup. The trimeric structure of the protein causes a step increase or decrease in the measured current corresponding to the opening or closing of a monomer. The current trace after insertion of multiple protein channels into the nano BLM at 100 mV in the presence of 0.5 M KCl, 10 mM HEPES at pH 7.4 is shown in Fig 37. The all-point conductance histogram of the current calculated from the time plot is shown in Fig. 38. A spacing of around 0.7 nS is seen between the peaks, corresponding to the opening of a single monomer. Sub-conductance states are also observed to exist from the time trace of the current. The current level is ~ 2150 pA in this trial. The current level differs in every trial depending on the number of open channels inserted and the number of pores covered with lipid bilayers obstructing ionic current through them.

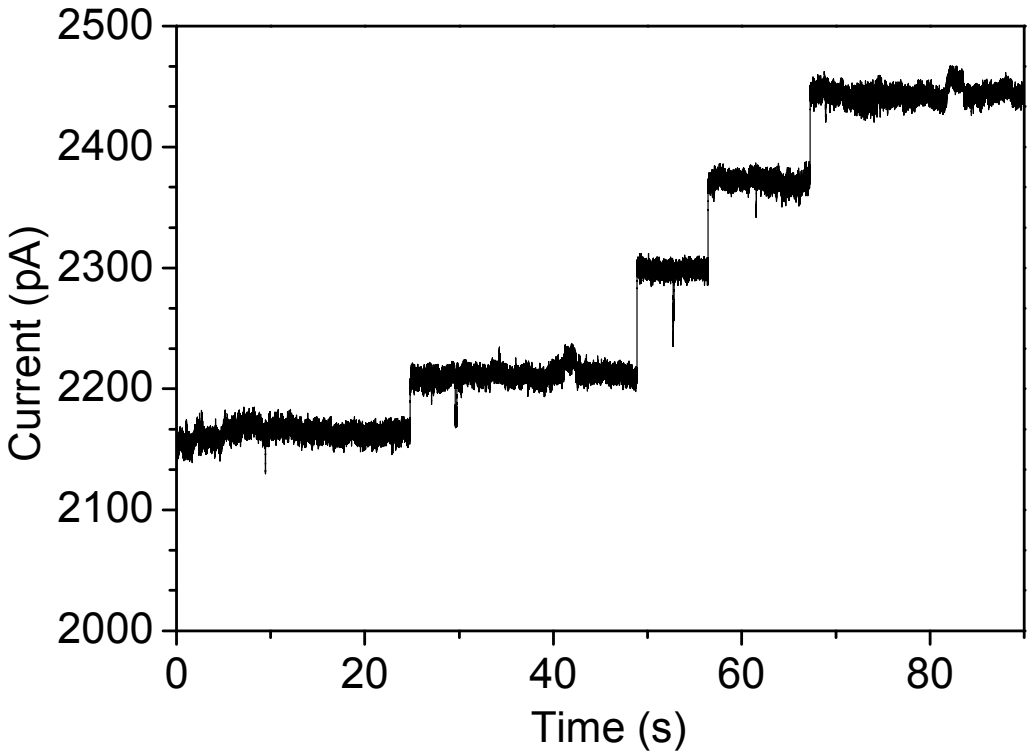

Figure 37: OmpF switching characteristics an applied voltage of 100 mV

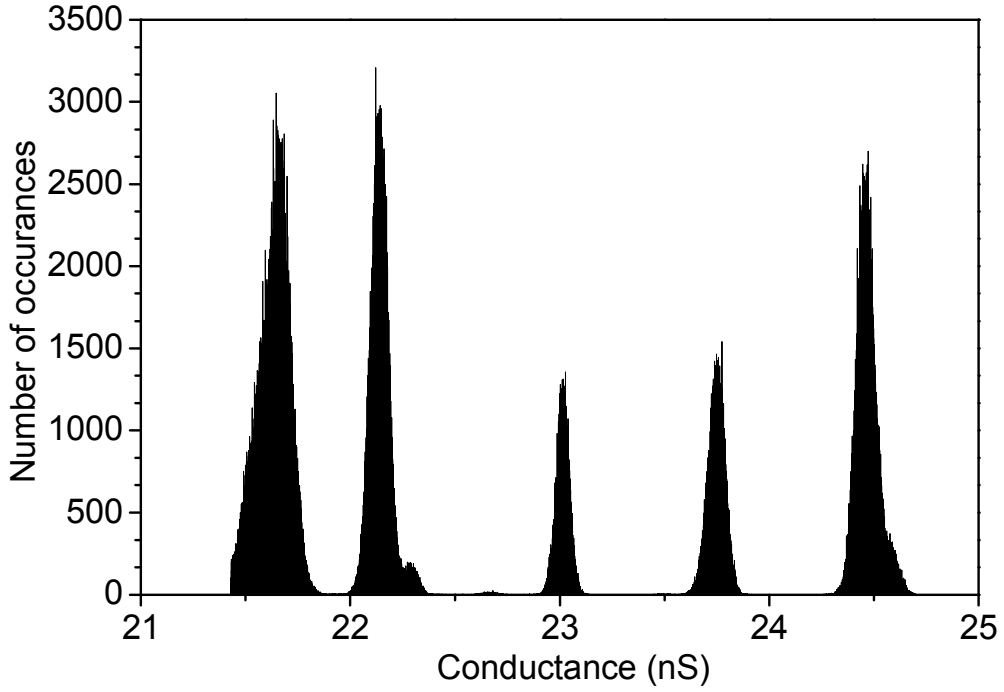

Figure 38: All-point histogram of switching characteristics of OmpF

CHAPTER 4

CONCLUSIONS

A simplified geometry of the smallest aperture of the diatom shell was used to simulate the ionic current as a function of the position of a polystyrene sphere in the aperture during a single translocation event. In addition, a mobility of 1.11 x 10^{-8} $m^2s^{-1}V^{-1}$ for the 27 nm polystyrene spheres was used to convert the simulated current from spatial dependence to time dependence in order to match the average experimental translocation time of 155 µs. It can be concluded from the results that a simplified single nanopore two-dimensional geometry can be used to predict the experimental and analytical current reduction within an error of 1.15 % and 5 % respectively.

The biogenic membranes could also be used to host lipid bilayer membranes with high membrane resistances to perform ion-channel recordings. The extreme hydrophilic nature of the diatom shells poses a challenge to host lipid bilayer membranes. This is indicated by the formation probability of 1 out of 10 on the non-functionalized pores. In the case of alumina nanopores found in literature, the surface was coated with gold and subsequently functionalized using thiol-chemistry rendering the surface hydrophobic (Romer and Steinem, Impedance analysis and single-channel recordings on nanoblack lipid membranes based on porous alumina 2004). In the case of Silicon Nitride nanopores, it is unclear if any surface modification was performed to make the surface hydrophobic (Studer, et al. 2009). A plasma-deposited PTFE approach to functionalize the surface cannot be used here as a 20 nm layer of PTFE is expected to line the pores (S. Wilk, L. Petrossian, et al. 2007). With a pore diameter of 40 nm the danger of clogging the pores is greatly increased. Additionally, rendering the inner surface of the pores hydrophobic can

also lead to difficulty in filling the pores with the electrolytic solution to establish electrical conductivity between the cis and trans compartments.

In this work, diatom shells functionalized with HMDS or 20 % TMCS in 1-Hexane yielded a formation probability of 10 out of 10. It is evident that a hydrophobic surface is necessary to successfully host nano-BLMs across a nanoporous substrate.

Impedance spectroscopy of diatoms functionalized with HMDS showed that a membrane resistance of close to 1 GΩ could be obtained. Repeatable formation of lipid bilayers was achievable and the nano-BLMs were stable for a few hours and gradually broke down. In case of TMCS functionalized diatoms, membrane resistances of more than 1 GΩ were achievable. By comparing the contact angles of ultrapure water on the nanoporous surface functionalized with HMDS and TMCS, it can be concluded that TMCS rendered better hydrophobicity to the surface, thereby forming membrane resistances > 1GΩ every time when a bilayer was formed. A comparison of results between bilayers formed on HMDS and TMCS functionalized diatoms shows that the degree of hydrophobicity of the surface plays a determinant role in bilayer formation and stability across nanoporous substrates. Therefore, it is not only the size of the pores but also the effective functionalization of diatoms that determines the formation of nano BLMs. The formation probability of 1 out of 10 in the non-functionalized diatom pores could be attributed to factors such as presence of residual organic material in the diatomic shell or use of the organic UV curable epoxy to immobilize the diatom shell on the silica substrate, which could render the surface in its vicinity hydrophobic, thereby assisting the formation of nano-BLMs.

The membrane capacitance values of the bilayers formed across the pores functionalized with TMCS were around 47 pF – 64 pF over several trials. The high capacitance indicates the presence of thin bilayers. The membrane parameters after the initial formation of bilayers can be observed over time in Fig. 18. The membrane capacitance when the bilayers were formed was around 52 pF. Over a period of 4 hours the capacitance value gradually increased to about 54 pF. The increase in the membrane capacitance indicates that the bilayers thin from the initial thickness at which they were formed.

The membrane resistance, on the other hand, decreased from 1.342 GΩ to 0.951 GΩ over a period of 3.5 hours. The gradual decrease in membrane resistance indicates that multiple bilayers were formed across the nanoporous membrane initially, which break down one by one gradually. In case a single bilayer had formed across the entire nanoporous surface, a break in the single lipid bilayer membrane would have led to a sudden decrease in the measured resistance, eventually leading one to measure the electrolytic resistance between the cis and the trans compartments. In this case however, the gradual decrease in the value of membrane resistance indicates that the breakdown of a single nano-BLM does not affect the other BLMs formed in parallel. In case of breakdown of one of the BLMs, an increase in the baseline current can be seen in the current-time trace owing to the open nanopore conducting between the trans and cis compartments. However, the other nano-BLMs that remain active are still useful for performing reconstitution experiments.

In the particular trial shown in Fig .30, the lifetime of the gigaseal formed was around 3.5 hours. The longest lifetime of gigaseal achieved with TMCS functionalized diatom was about 15 hours shown in Fig. 32. In this case, the initial membrane resistance was 2.403 GΩ. The corresponding membrane capacitance was measured to be 64.1 pF

indicating that it was a thin bilayer. In 12 hours, the membrane resistance changed to 1.784 GΩ and the membrane capacitance was measured to be 58.6 pF. This indicates that the bilayer thickness had increased from the initial thickness. However, this value is still comparable to previous trials ranging from 52 – 54 pF. After 15 hours of time the measured membrane resistance was 72.2 MΩ. The resistance of the open diatom without addition of lipids was in the range of hundreds of 100 kΩ to 5 MΩ. The high value of 72.2 MΩ indicates that majority of the nano-BLMs had ruptured leaving a few intact.

The bilayer structure of the lipid membrane across the nanopores and their suitability to perform ion-channel reconstitution experiments was checked by recording the transmembrane currents after self-insertion of OmpF protein. Characteristic activities of the membrane protein OmpF were recorded after insertion into the nano-BLM at 100 mV. Conductance steps of 0.7 nS in 0.5 M KCl corresponding to the conductance of a single monomeric unit can be seen in the current trace. In addition, sub-conductance states of the protein < 0.7 nS were recorded. A single channel conductance of 0.7 nS is commonly reported in literature for the OmpF porin in 0.5 M KCl (Schindler and Rosenbusch 1978) (Schirmer 1998) (Van der straaten, et al. 2003) (Wilk, Aboud, et al. 2006). The current levels for each experiment however were different because of two factors namely, number of open ion channels inserted and number of active nano-BLMs existing across the nanopores. The insertion and channel activity confirms the existence of nano-BLMs, as it is well established that physiological OmpF activity can only be observed in lipid bilayers and not in lipid multilayers.

REFERENCES

Adiga, S. P., C. Jin, L. A. Curtiss, N. A. Monteiro-Riviere, and R. J. Narayan. 2009. "Nanoporous membranes for medical and biological applications." Wiley Interdiscip Rev Nanomed Nanobiotechnol. 1(5): 568–581. doi:doi:10.1002/wnan.50.

Agrawal, A. A. , B. J. Nehilla, K. V. Reisig, T. R. Gaborski, D. Z. Fang, C. C. Striemer, P. M. Fauchet, and J. M. McGrath. 2010. "Porous nanocrystalline silicon membranes as highly permeable and molecularly thin substrates for cell culture." Biomaterials 31: 5408 - 5417.

Alfredo de la Escosura-Muñiz, and Arben Merkoçi. 2012. "Nanochannels Preparation and Application in Biosensing." ACS Nano 6(9): 7556 - 7583. doi:10.1021/nn301368z.

Anderson, R. C. , Muller, R. S. , and Tobias, C. W. 1993. "Chemical Surface Modification of Porous Silicon." Journal of Electrochemical Society 1393-1396.

Andersson, M. , H. M. Keizer, C. Zhu, D. Fine, A. Dodabalapur, and R. S. Duran. 2007. "Detection of Single Ion Channel Activity on a Chip Using Tethered Bilayer Membranes." Langmuir 23 (6): 2924 - 2927.

Atanasov, V. , N. Knorr, R. S. Duran, S. Ingebrandt, A. Offenhäusser, W. Knoll, and I. Köper. 2005. "Membrane on a Chip: A Functional Tethered Lipid Bilayer Membrane on Silicon Oxide Surfaces." Biophysical Journal 89 (3): 1780 - 1788.

Bao, Z. H., M.R. Weatherspoon, S. Shian, Y. Cai, P.D. Graham, S.M. Allan, G. Ahmad, et al. 2007. "Chemical reduction of three-dimensional silica micro-assemblies into microporous silicon replicas." Nature 446: 172 - 175.

Bayley, H. , and P. S. Cremer. 2001. "Stochastic sensors inspired by biology." Nature 413: 226 - 230.

Boyd, C. M., and D. Gradmann. 1999. "Electrophysiology of the marine diatom Coscinodiscus wailesii I. Endogenous changes of membrane voltage and resistance." Journal of Experimental Botany 50 (333): 445 - 452.

Bozarth, A., U. G. Maier, and S. Zauner. 2009. "Diatoms in biotechnology: modern tools and applications." Applied Microbiology and Biotechnology 82: 195 - 201.

Butler, T. Z. , M. Pavlenok, I. M. Derrington, M. Niederweis, and J. H. Gundlach. 2008. "Single-molecule DNA detection with an engineered MspA protein nanopore." Proceeedings of the National Academy of Sciences of the United States of America 105: 20647-20652.

Castellana, E.T., Cramer, P.S. 2006. "Solid supported lipid bilayers: From biophysical studies to sensor design." Surface Science reports 61: 429 - 444.

Coakley, K. M., B. S. Srinivasan, J. M. Ziebarth, C. Goh, Y. Liu, and M. D. McGehee. 2005. "Enhanced hole mobility in regioregular polythiophene infiltrated in straight nanopores." Advanced Functional Materials 15: 1927 - 32.

Desai, T. A., D. J. Hansford, L Kulinsky, A. H. Nashat, G. Rasi, J. Tu, Y. Wang, M. Zhang, and M. Ferrari. 1999. "Nanopore Technology for Biomedical Applications." Biomedical Microdevices 2 (1): 11 - 40.

G., Schmid. 2002. "Materials in nanoporous alumina." J. Mater. Chem. 12: 1231 - 1238.

Gassmann, O., M. Kreir, C. Ambrosi, J. Pranskevich, A. Oshima, C. Roling, G. Sosinsky, N. Fertig, and C. Steinem. 2009. "The M34A mutant of Connexin26 reveals active conductance states in pore-suspending membranes." Journal of structural biology 168: 168 - 76.

Gordon, R., and R.W. Drum. n.d. "The chemical basis for diatom morphogenesis." International Review of Cytology I50: 243 - 372.

Gordon, R., D. Losic, M. A. Tiffany, S. S. Nagy, and F. A. S. Sterrenburg. 2009. "The Glass Menagerie: diatoms for novel applications in nanotechnology." Trends in Biotechnology 27: 116 - 127.

Goryll, M., Chaplot, N. 2009. "Miniaturized silicon apertures for lipid bilayer reconstitution experiments." Proceedings of Material Research Society 1191.

Goyne, K. W., A. R. Zimmerman, B. L. Newalkar, S. Komarneni, S. L. Brantley, and J. Chorover. 2002. "Surface Charge of Variable Porosity Al2O3(s) and SiO2(s) Adsorbents." Journal of Porous Materials 9: 243–256.

Hamill, O.P., Sakmann B. 1980. "A cell-free method for recording single-channel currents from biological membranes." Proceedings of Physiological Society 41.

HEKA. n.d. HEKA EPC 7, EPC 8, EPC 8 plus patch clamp amplifier manual.

Henriquez, R. R. , Ito, T. , Sun, L. , Crooks, R. M. 2004. "The resurgence of Coulter counting for analyzing nanoscale objects." The Royal Society of Chemistry 129: 478-482.

Howorka, S. , and H. Bayley. 2002. "Probing distance and electrical potential within a protein pore with tethered DNA." Biophysical Journal 83: 3202 - 3210.

Howorka, S. , and Z. Siwy. 2009. "Nanopore analytics: sensing of single molecules." Chemical Society Review 38: 2360-2384.

Jane, A., R. Dronov, A. Hodges, and H. N. Voelcker. 2009. "Porous silicon biosensors on the advance." Trends in Biotechnology 27 (4): 230 - 239.

Jani, A. M. M., J. Zhou, M. R. Nussioa, D. Losic, J. G. Shapter, and N. H. Voelcker. 2008. "Pore spanning lipid bilayers on silanised nanoporous alumina membranes." Proc. of SPIE 7267. doi:doi: 10.1117/12.808769.

Jeffryes, C., R. Solanki, Y. Rangineni, W. Wang, C.H. Chang, and G.L. Rorrer. 2008. "Electroluminescence and photoluminescence from nanostructured diatom frustules containing metabolically inserted germanium." Advanced Materials 20: 2633-2637.

Jeffryes, C., T. Gutu, J. Jiao, and G.L. Rorrer. 2008. "Metabolic Insertion of Nanostructured TiO2 into the Patterned Biosilica of the Diatom Pinnularia sp by a Two-Stage Bioreactor Cultivation Process." Acs Nano 2: 2103-2112.

Jubery, T. Z., A. S. Prabhu, M. J. Kim, and P. Dutta. 2012. "Modeling and simulation of nanoparticle separation through a solid-state nanopore." Electrophoresis 33: 325 - 333.

Khung, Y. L., G. Barritt, and N. H. Voelcker. 2008. "Using continuous porous silicon gradients to study the influence of surface topography on the behaviour of neuroblastoma cells." Experimental Cell Research 314: 789 - 800.

Kim, M. J., M. Wanunu, D. C. Bell, and A. Meller. 2006. "Rapid Fabrication of Uniformly Sized Nanopores and Nanopore Arrays for Parallel DNA Analysis." Advanced Materials 18: 3149 - 3153.

Komarov, F. F., L. A. Vlasukova, O. M. Milchanin, P. I. Gaiduk, V. N. Yuvchenko, and S. S. Grechnyi. 2005. "Ion-beam formation of nanopores and nanoclusters in SiO2." Vacuum 78: 361 - 366.

Kra¨mer, E, S Fo¨rster, C Go¨ltner, and M Antonietti. 1998. "Synthesis of Nanoporous Silica with New Pore Morphologies by Templating the Assemblies of Ionic Block Copolymers." Langmuir 14: 2027 - 2013.

Krishna, G. , J. Schulte, B. A. Cornel, R. J. Pace, and P. D. Osman. 2003. "Tethered Bilayer Membranes Containing Ionic Reservoirs: Selectivity and Conductance." Langmuir 19 (6): 2294 - 2305.

Kroeger, N., and N. Poulsen. 2008. "Diatoms—From Cell Wall Biogenesis to Nanotechnology." Annual Review of Genetics 42: 83 - 107.

L. X. Tiefenauer and A. Studer. 2008. "Nano for bio: Nanopore arrays for stable and functional lipid bilayer membranes (Mini Review)." Biointerphases Journal 3: 74-79.

Lan, W.-J., D. A. Holden, B. Zhang, and H. S. White. 2011. "Nanoparticle Transport in Conical-Shaped Nanopores." Analytical Chemistry 83: 3840 - 3847.

Launer, P. J. 1987. Infrared analysis of Organosilicon compounds: Spectra Structure Correlations. New york: Laboratory for Materials, Inc.

Lin, K.C., V. Kunduru, M. Bothara, K. Rege, S. Prasad, and B.L. Ramakrishna. 2010. "Biogenic nanoporous silica-based sensor for enhanced electrochemical detection of cardiovascular biomarkers proteins." Biosensors and bioelectronics 25: 2336 - 2342.

Liu, H., S. Qian, and H. H. Bau. 2007. "The effect of translocating cylindrical particles on the ionic current through a nanopore." Biophysical Journal 92: 1164 - 1177.

Lo, C. J., T. Aref, and A. Bezryadin. 2006. "Fabrication of symmetric sub-5 nm nanopores using focused ion and electron beams." Nanotechnology 17: 3264 - 3267.

Losic, D., G. Rosengarten, J. G. Mitchell, and N. H. Voelcker. 2006. "Pore architecture of diatom frustules: potential nanostructured membranes for molecular and particle separations." Journal of Nanoscience and Nanotechnology 6: 982-9.

Losic, D., J. G. Mitchell, and N. H. Voelcker. 2009. "Diatomaceous lessons in nanotechnology and advanced materials." Advanced Materials 21: 2947–2958.

Losic, D., Mitchell J.G., and N.H. Voelcker. 2008. "Diatom culture media contain extracellular silica nanoparticles which form opalescent films." SPIE Proceedings, Smart Materials V 7267.

Mahadik, D. B. , Rao, A. V. , Rao , A. P. , Wagh, P. B. , Ingale, S. V. , Gupta, S. C. 2011. "Effect of concentration of trimethylchlorosilane (TMCS) and hexamethyldisilazane (HMDZ) silylating agents on surface free energy of silica aerogels." Journal of Colloid and Interface Science 298-302.

Masuda, H., H. Yamada, M. Satoh, H. Asoh, M. Nakao, and T. Tamamura. 1997. "Highly ordered nanochannel-array architecture in anodic alumina." Appl. Phys. Lett. 71: 2770 - 72.

Mayer, M. , J. K. Kriebel, M. T. Tosteson, and G. M. Whitesides. 2003. "Microfabricated Teflon Membranes for Low-Noise Recordings of Ion Channels in Planar Lipid Bilayers." Biophysical Journal 85: 2684–2695.

Neher, E., Sakmann, B. 1976. "Single channel currents recorded from membrane of denervated frog muscle fibres, NATURE, Vol. 260, 799 - 802. (1976). Single channel currents recorded from membrane of denervated frog muscle fibres." Nature 260: 799 - 802.

Niles, W.D., Levis, R.A., Cohen, F.S. 1988. "Planar bilayer membranes made from phospholipid monolayers form by a thinning process." Biophysical Journal 53: 327 - 335.

Nishizawa, M. , V. P. Menon, and C. R. Martin. 1995. "Metal Nanotubule Membranes with Electrochemically Switchable Ion-Transport Selectivity." Science 268: 700 - 702.

Osaki, T., Suzuki, H., Pioufle, B.L., Takeuchi, S. 2009. "Multichannel Simultaneous Measurements of Single-Molecule Translocation in α -Hemolysin Nanopore Array." Analytical Chemistry 81 (24): 9866 - 9870.

Parkinson, J., and R. Gordon. 1999. "Beyond micromachining: the potential of diatoms." Trends in Biotechnology 17 (5): 190 - 196.

Prasad, S., and J. Quijano. 2006. "Development of nanostructured biomedical micro-drug testing device based on in situ cellular activity monitoring." Biosensors and Bioelectronics 21: 1219–1229.

Purnell, R. F. , and J. J. Schmidt. 2009. "Discrimination of Single Base Substitutions in a DNA Strand Immobilized in a Biological Nanopore." ACS Nano 3: 2533-2538.

Purnell, R. F. , K. K. Mehta, and J. J. Schmidt. 2008. "Nucleotide identification and orientation discrimination of DNA Homopolymers immobilized in a protein nanopore." Nano letters 8: 3029 - 3034.

Qin, T., T. Gutu, J. Jiao, C.H. Chang, and G.L. Rorrer. 2008. "Biological fabrication of photoluminescent nanocomb structures by metabolic incorporation of germanium into the biosilica o the diatom Nitzschia frustulum." Acs Nano 2: 1296-1304.

Rapp, B. 2004. "Manipulating diatoms." Materials Today 13.

Romer, W. , and C. Steinem. 2004. "Impedance analysis and single-channel recordings on nano-black lipid membranes based on porous alumina." Biophysical Journal 86: 955 - 65.

Romer, W., and C. Steinem. 2004. "Impedance analysis and single-channel recordings on nanoblack lipid membranes based on porous alumina." Biophysical Journal 86: 955-65.

Sakmann, B., Neher, E. 1995. Single channel recording. New York: Plenum Press.

Schindler, H., and J. P. Rosenbusch. 1978. "Matrix protein from Escherichia coli outer membranes forms voltage-controlled channels in lipid bilayers." Proc. Nati. Acad. Sci. 75: 3751 - 3755.

Schirmer, T. 1998. "General and Specific Porins from Bacterial Outer Membranes." Journal of Structural Biology 121: 101 - 109.

Schmitt, E.K., M. Vrouenraets, and C. Steinem. 2006. "Channel activity of OmpF monitered in nano-BLMs." Biophysical Journal 91: 2163-71.

Schumann, S., S. A. F. Bon, R. A. Hatton, and T. S. Jones. 2009. "Open-cellular organic semiconductor thin films by vertical co-deposition using sub-100 nm nanosphere templates." Chemical Communitcations 6478 - 6480.

Sigworth, F.J. 1995. "Design of the EPC-9, a computer-controlled patch-clamp amplifier. 1. Hardware." Journal of Neuroscience Method 56: 195 - 20.

Striemer, C. C., T. R. Gaborski, J. L. McGrath, and P. M. Fauchet. 2007. "Charge- and size-based separation of macromolecules using ultrathin silicon membranes." Nature Letters 445: 749 - 753.

Studer, A, X Han, F. K. Winkler, and L.X. Tiefenauer. 2009. "Formation of individual protein channels in lipid bilayers suspended in nanopores." Colloids and Surfaces B: Biointerfaces 73: 325–331.

Takoh, K., T. Ishibashi, T. Matsue, and M. Nishizawa. 2005. "Localized chemical stimulation of cellular micropatterns using a porous membrane-based culture substrate." Sensors and Actuators B-Chemical 108: 683 - 687.

Umemura, K., X. Liao, S. Mayama, and K. M. Gad. 2007. "Controlled nanoporous structures of a marine diatom." Journal of nanoscience and Nanotechnology 7: 2842 - 2846.

Van der straaten, T.A., J.M. Tang, U. Ravaioli, R.S. Eisenberg, and N.R. Aluru. 2003. "Simulating Ion Permeation Through the ompF Porin Ion Channel Using Three-Dimensional Drift-Diffusion Theory." Journal of Computational Electronics 2: 29-47.

Vasileska, D. and Goodnick, S. M. 2006. Computational Electronics. Morgan and Claypool.

Vlassiouk, I., P. Y. Apel, S. N. Dmitriev, K. Healya, and Z. S. Siwy. 2009. "Versatile ultrathin nanoporous silicon nitride membranes." Proceedings of the National Academy of Sciences 106 (50): 21039 - 44.

Vlassiouk, I., S. Smirnov, and Z. Siwy. 2008. "Ionic Selectivity of Single Nanochannels." Nanoletters 8: 1978 - 1985.

Vockenroth, I. K., P. P. Atanasova, A. Toby, A. Jenkins, and I. Köper. 2008. "Incorporation of α-Hemolysin in Different Tethered Bilayer Lipid Membrane Architectures." Langmuir 24 (2): 496 - 502.

Ward, R.K., S. Mungall, J. Carter, and R.H. Clothier. 1997. "Evaluation of tissue culture insert membrane compatibility in the fluorescein leakage assay." Toxicology in vitro 11: 761-768.

Wee, K. M., T. N. Rogers, B. S. Altan, and S. A. Hackne. 2005. "Engineering and medical applications of diatoms." Journal of Nanoscience and Nanotechnology 5: 88 - 91.

White, R. J. , E. N. Ervin, T. Yang, X. Chen, S. Daniel, P. S. Cremer, and H. S. White. 2007. "Single Ion-Channel Recordings Using Glass Nanopore Membranes." Journal of American Chemical Society 129: 11766-11775.

Wilk, S. 2005. Dissertation on Microfabricated silicon apertures for transmembrane ion channel measurement. Arizona State University.

Wilk, S. J., L. Petrossian, M. Goryll, T. J. Thornton, S. M. Goodnick, J. M. Tang, and R. S. Eisenberg. 2007. "Integrated electrodes on a silicon based ion channel measurement platform." Biosensors and Bioelectronics 23: 183-190.

Wilk, S.J., L. Petrossian, M. Goryll, T.J. Thornton, S.M. Goodnick, J.M. Tang, and R.S. Eisenberg. 2007. "Integrated electrodes on a silicon based ion channel measurement platform." Biosensors and Bioelectronics 23: 183–190.

Wilk, S.J., M. Goryll, G.M. Laws, S.M. Goodnick, T.J. Thornton, M. Saraniti, and J. Tang. 2004. "Teflon™-coated silicon apertures for supported lipid bilayer membranes." Applied Physics Letters 85: 3307 - 3309.

Wilk, S.J., S. Aboud, L. Petrossian, M. Goryll, J.M. Tang, R.S. Eisenberg, M. Saraniti, S.M. Goodnick, and T.J. Thornton. 2006. "Ion Channel Conductance Measurements on a Silicon-Based Platform." Journal of Physics: Conference Series 38: 21 - 24.

Wu, M.-Y., D. Krapf, M. Zandbergen, H. Zandbergen, and P. E. Batson. 2005. "Formation of nanopores in a SiN/SiO2 membrane with an electron beam." Applied Physics Letters 87: 113106 - 1.

Yu, Y., J. Addai-Mensah, and D. Losic. 2012. "Functionalized diatom silica microparticles for removal of mercury ions." Science and Technology of Advanced materials 13: 1 - 11.

Yusko, E. C., Johnson, J. M., Majd, S., Prangkio, P., Rollings, R.C., Li, J., Yang, J., Mayer, M. 2011. "Controlling protein translocation through nanopores with bio-inspired fluid walls." Nature nanotechnology 253 - 260.

Zhang, D., Y. Wang, and J. Pan. 2010. "Separation of diatom valves and girdle bands from Coscinodiscus diatomite by settling method." Journal of Material Sciences 45: 5736–5741.

Zhao, Q., Wang, D., Jayawardhana, D.A, Guan, X. 2008. "Stochastic sensing of biomolecules in a nanopore sensor." Nanotechnology 19 (50).